Sensitivity of a Coupled Single-Column Model in the Tropics to Treatment of the Interfacial Parameterizations

CAROL ANNE CLAYSON AND AIDONG CHEN

Department of Earth and Atmospheric Sciences, Purdue University, West Lafayette, Indiana

(Manuscript received 27 August 2001, in final form 13 December 2001)

ABSTRACT

A coupled atmosphere–ocean single-column model has been developed for testing tropical ocean–atmosphere feedbacks. The model is evaluated against observational data (both in situ and satellite) during the Tropical Ocean Global Atmosphere Coupled Ocean–Atmosphere Response Experiment (TOGA COARE) intensive observation period. The coupled model is able to successfully reproduce variations in cloud parameters and surface fluxes; the model also overestimates the latent and sensible heat fluxes compared to observations. The overestimation is most likely due to errors in the atmospheric surface layer temperature and specific humidity. The sea surface temperatures produced by the model are reasonable. The mean bias in sea surface temperature as compared to buoy data is 0°C; the maximum deviation from the observed temperature is 0.4°C.

This model is then used to investigate the sensitivity of the ocean and the ocean–atmosphere system to variations in the included interfacial parameterization in the tropical Pacific. The sensitivity of the model results to the turbulent flux model used in the coupled version is shown to produce daily averaged sea surface temperature variations of over 0.5°C. Of equal significance is the variation in model response to temperatures from different depths in the water column. Use of the typically cooler skin temperature as the interfacial temperature rather than the temperature at depth results in strong differences in the atmospheric profiles of heat, moisture, and cloud properties. These differences are not caused solely by the difference in temperature, but are also due to the much-reduced diurnal variation in sea surface temperature at depth. The extent to which a daily averaged sea surface temperature changes the resulting atmospheric profiles depends on whether the diurnal variability was strong; under low-wind conditions the differences are the most dramatic.

1. Introduction

Interactions between the tropical atmosphere and ocean have now been established to be of fundamental importance to the evolution of the El Niño–Southern Oscillation (ENSO), intraseasonal oscillations such as the Madden–Julian oscillation (MJO), and monsoons (e.g., Philander et al. 1984; Neelin 1991; Webster et al. 1998; Wang and Xie 1998). Experiments using atmospheric general circulation models (e.g., Palmer and Mansfield 1984; Shukla 1998) have shown that the atmospheric circulation is very sensitive to small changes in sea surface temperature (SST) in the tropical western Pacific Ocean warm pool region. At the same time, the SST and the ocean mixed layer structure in the warm pool are very sensitive to changes in the surface heat, momentum, and freshwater fluxes that are driven by the atmospheric circulation. The mutual sensitivity of the ocean and the atmosphere in the warm pool region places stringent requirements on models of the coupled ocean–atmosphere system, and coupled climate simulations commonly show significant drift in sea surface temperature if the surface fluxes are not forced toward climatology. In spite of these model sensitivities, observations show that the warm pool SST remains remarkably constant, showing variations of only a few degrees even during the last glaciation (see Webster 1994 for a review). In view of the small range of surface temperatures observed, it appears that negative feedbacks are active to stabilize the tropical ocean surface temperature. The nature of the negative feedbacks in this region continues to be hotly debated.

This study addresses the local thermodynamic interactions between the atmosphere and upper ocean in the warm pool. The interaction between the tropical atmosphere and the Pacific Ocean warm pool consists of intense but episodic exchanges of heat, momentum, and freshwater. We focus specifically on short timescale atmosphere–ocean interactions. Several aspects of high-frequency air–sea interactions have been explored using the Tropical Ocean Global Atmosphere Coupled Ocean–Atmosphere Response Experiment (TOGA COARE) dataset (Webster and Lukas 1992; Godfrey et al. 1998) along with cloud-resolving models (a few of which have been coupled to an ocean mixed layer model), including

Corresponding author address: Carol Anne Clayson, Department of Earth and Atmospheric Sciences, Purdue University, 1397 CIVL Building, West Lafayette, IN 47907-1397.
E-mail: clayson@purdue.edu

Wang et al. (1996), Lau and Sui (1997), Feng et al. (1998), and Li et al. (1998). Fasullo and Webster (1999) studied surface heat flux anomalies over the tropical Indian and Pacific Oceans and compared them with changes in SST during warming events. They concluded that the maintenance of the warm pool SST requires both local interactions and large-scale dynamic systems. Outstanding issues that still remain in improving the simulation of the high-frequency air–sea interaction in the tropical western Pacific include the following: the effects of precipitation on the ocean and its response back to the atmosphere (e.g., Zhang et al. 2000); the role of short timescale-type events on the thermodynamic coupling between the ocean and atmosphere, such as the coupling between the ocean mixed layer and the atmosphere on MJO timescales (e.g., Wang and Xie 1998); and the role of short timescale variability such as 2–3-day oscillations on the coupled ocean–atmosphere system (e.g., Chen et al. 1996; Clayson et al. 2002).

Given the apparent sensitivity of the tropical climate system to small variations in SST (and resultant variations in surface fluxes), much work has been devoted to understanding the mechanisms by which the interfacial (or skin) temperature differs from temperatures below. Several models of the bulk–skin temperature difference based on surface renewal have been formulated. In addition, a number of models for determining the surface turbulent flux exchange between the ocean and the atmosphere have been formulated, including Fairall et al. (1996a), Clayson et al. (1996), Smith (1988), and Bourassa et al. (1999). Recently Brunke et al. (2001, manuscript submitted to *J. Geophys. Res.*, hereafter BZA) have evaluated the differences between these models and found that long-term differences in latent heat fluxes can be on the order of 20 W m^{-2}. A goal of researchers in the tropical Pacific has been to produce a net heat flux with biases of less than 10 W m^{-2} (Webster and Lukas 1992), based in part on ocean model simulations conducted by Seager et al. (1988) and Gent (1991), who have shown that net surface heat flux differences of 10 W m^{-2} in the tropical western Pacific can change the modeled SST by 1°C over a 1-yr period. It is still unclear as to what effects changes in surface fluxes over these ranges have on the coupled atmosphere–ocean system, especially over short timescales.

This study extends the previous research on short-term air–sea interactions during TOGA COARE by using observed and modeled data to evaluate the effects of interfacial parameterizations on the coupled system in the tropical Pacific. In order to address the thermodynamic coupling of the ocean–atmosphere system in the western Pacific, this study compares a coupled single-column atmosphere–ocean model with standard meteorological and observational data, and then evaluates the variability of the model results dependent upon the use of various bulk and skin temperatures as the interface temperature and variations associated with differing flux models.

The single-column model (SCM) is a single vertical array of cells from a three-dimensional climate model that is forced externally by advective tendencies (Randall et al. 1996). The single-column model has been used extensively as a tool to evaluate and improve model parameterizations (e.g., Betts and Miller 1986; Bechtold et al. 2000, manuscript submitted to *Quart. J. Roy. Meteor. Soc.*). In the study of the tropical atmosphere and ocean, single-column model studies have included Randall et al. (1996) and Iacobellis and Somerville (2000). Because the large-scale advective tendencies are specified, SCMs cannot reveal the interactions of parameterized processes with the large-scale dynamics. However, using the SCM allows isolation of the local, thermodynamic interactions, which is useful for understanding the local thermodynamic interactions between the atmosphere and ocean, and also in evaluating the relevant physical parameterizations. The atmospheric and oceanic components of the coupled model and the coupling of these components are described, and comparisons of the results with observed values during the TOGA COARE intensive observation period (IOP) are shown. Differences between model simulations of the four-month IOP that occur from the use of different sea surface temperature values and flux models are discussed, and these results are interpreted in order to gain understanding of the manner in which the coupled model responds to these various parameterizations.

2. Model description

The model used here consists of a coupled atmosphere–ocean single-column model. Simulations are conducted for the separate atmosphere and ocean models, as well as with the coupled model.

a. Ocean mixed layer model

The ocean component of the coupled model consists of the one-dimensional ocean described by Kantha and Clayson (1994) and Kantha and Clayson (2001, manuscript submitted to *Ocean Modelling*). This model uses second-moment turbulence closure, and includes improved parameterizations of the pressure covariance terms that have been developed based on large eddy simulations. The model includes the skin surface temperature parameterization developed by Wick (1995), modified by Schlüssel et al. (1997) to include the effects of precipitation and the diurnal thermocline. Parameterizations for Langmuir circulation and wave breaking effects have also been included. The ocean mixed layer model has been evaluated over many timescales and in many locations, including data from the TOGA COARE pilot cruise (Kantha and Clayson 1994) and the IOP (Webster et al. 1996). Comparisons of the model turbulence characteristics including dissipation have been

validated against data from the R/V *Moana Wave* during the IOP (Clayson and Kantha 1999). The vertical resolution of the ocean model is 1 m; temporal resolution is 15 min. The profiles of temperature, salinity, and currents used to initialize the model are described in the following section.

The horizontal and vertical advection of heat and salt are calculated from the results of a three-dimensional ocean model. The model is the University of Colorado version (CUPOM) of the Princeton sigma-coordinate, free-surface, 3D ocean model (Blumberg and Mellor 1987) configured for the tropical Pacific Ocean (Clayson 1995), which incorporates the mixed layer model described above. The tropical Pacific version of the model has a fine horizontal resolution (1/3° in the zonal direction) in the western Pacific warm pool region, changing to a fairly coarse resolution (1° in the zonal direction) in the eastern and central Pacific. The resolution in the meridional direction is 1/3° in regions close to the equator telescoping to 1° at the edge of the model domain (20°N, 20°S). This version of the model is run at a fine vertical resolution (38 levels with 10-m resolution in the upper 250 m, less than 1 m near the surface) to resolve the mixed layer and the equatorial undercurrent. The tropical Pacific Ocean version of the model was initialized with data from the TOGA Tropical Atmosphere Ocean (TAO) array where available and with temperature and salinity data from Levitus (1984) when not available. Surface forcing is provided by a satellite dataset (Curry et al. 1999) that is available for the TOGA COARE IOP over the intensive flux array (IFA) region (from 4°S to 2°N and 150° to 160°E), with a spatial scale of 50 km and a temporal scale of 3 h (see section 3c for a full description). Locations outside this domain are forced with surface fluxes of heat, moisture, and momentum from the European Centre for Medium-Range Weather Forecasts (ECMWF) reanalysis dataset. These analyses are available 4 day^{-1} at a spatial resolution of 2.5°. Horizontal advection is calculated along the IFA boundary every 3 h.

b. Atmospheric model

The atmospheric component of the model used for this study is the single-column version of the National Center for Atmospheric Research (NCAR) Community Climate Model (CCM3; Kiehl et al. 1996) known as SCCM 1.2. The SCCM 1.2 is a one-dimensional time-dependent model in which the local time rate of change of the large-scale state variables of temperature, moisture, momentum, cloud water, etc., depends on specified horizontal flux divergences, a specified vertical motion field (from which the large-scale vertical advection terms are evaluated), and subgrid-scale sources, sinks, and eddy transports. The subgrid-scale contributions are determined by the model parameterizations of the relevant physical processes. The SCCM 1.2 contains physical parameterizations that are identical to those used in the full-scale CCM3. The SCM has 18 vertical levels, with a rigid lid at 2.917 mb. The model uses a time step of 15 min.

The atmospheric boundary layer parameterization uses the nonlocal scheme described by Holtslag and Boville (1993). This scheme determines an eddy-diffusivity profile based on a diagnosed boundary layer height (following Vogelezang and Holtslag 1996) and a turbulent velocity scale. It also includes nonlocal vertical transport effects for heat and moisture, and a direct coupling to the parameterization of deep and shallow convection.

The convection scheme used in SCCM 1.2 is the Zhang–McFarlane convection scheme (Zhang and McFarlane 1995). The cloud fraction in CCM3 is based on the Slingo (1987) algorithm as modified by Hack et al. (1993). This algorithm calculates convective cloud amount as a function of convective overturning. We have modified the SCCM 1.2 by replacing this scheme with the Tiedtke (1993) parameterization for cloud amount. In the Tiedtke parameterization, the area with convective updrafts is also considered to be convective cloud; the fractional area covered by these convective updrafts is parameterized by using the grid-averaged precipitation rate generated in each layer by the Zhang–McFarlane scheme (P_{ZM}). Using the precipitation rate formula of Sundqvist et al. (1989)

$$P_{\mathrm{ZM}} = \frac{a_u l_u}{c_{\mathrm{o}}}\left\{1 - \exp\left[-\left(\frac{l_u}{l_{\mathrm{crit}}}\right)^2\right]\right\} \tag{1}$$

the fractional area (a_u) of the updrafts can be solved for where l_u is the liquid water/ice within the updrafts, l_{crit} is a cloud water content at which the precipitation process becomes efficient, and c_o^{-1} is a characteristic timescale for conversion of cloud droplets into raindrops. This scheme has been used in the single-column model of Iacobellis and Somerville (2000) and was shown to provide greatly improved simulations of cloud parameters during the TOGA COARE IOP.

The method for determining the cloud water and cloud radiative properties in this coupled model has been altered from the CCM3 in that cloud optical properties are now calculated as a function of the cloud water path and the effective cloud droplet radius. In the original scheme, the cloud drop effective radius for liquid water clouds ($r_{e,l}$) is set to be 10 μm over the ocean. The ice particle effective radius ($r_{e,i}$) is a function of normalized pressure, and is set to be 10 μm for low clouds. In the new model, following Iacobellis and Somerville (2000), the effective cloud droplet radius is determined for a liquid water content (LWC) from

$$r_{e,l} = 100\left(\mathrm{LWC} \times \frac{3}{4\pi N}\right)^{1/3}. \tag{2}$$

LWC is the liquid water content (in g m^{-3}); N is the droplet number concentration, taken as 600 cm^{-3} from

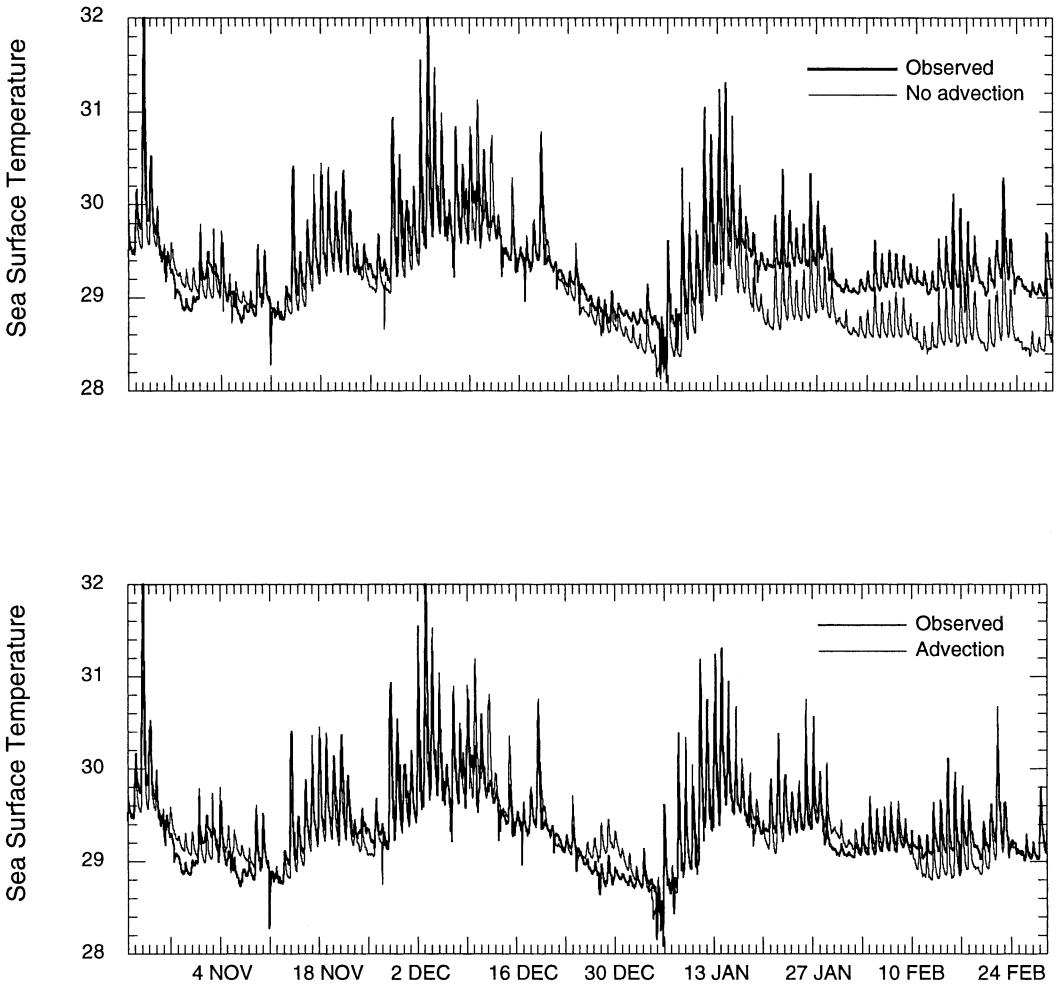

FIG. 1. Observed and modeled SSTs. (top) Model data is from the stand-alone ocean model with no advection and the IMET buoy data for 21 Oct as the initial profile, and (bottom) the stand-alone ocean model with advection and the IMET buoy data for 21 Oct as the initial profile.

Bower et al. (1994); $r_{e,l}$ is in μm. The effective cloud droplet radius for ice clouds is

$$r_{e,i} = 0.71T + 61.29 \tag{3}$$

based on the estimate of Suzuki et al. (1993), where $r_{e,i}$ is in μm and T is in °C. For clouds with a combination of ice and liquid water, Iacobellis and Somerville (2000) use

$$r_e = f_L r_{e,l} + (1 - f_L) r_{e,i} \tag{4}$$

for the definition of the effective cloud droplet radius, where f_L is the fraction of liquid cloud water based on the formula of Smith (1990):

$$f_L = \frac{1}{6}\left(\frac{T + 15}{5}\right)^2 \quad \text{for } -15°\text{C} < T \leq -5°\text{C}$$

$$f_L = \frac{1}{3}\left(\frac{T}{5}\right)^2 \quad \text{for } -5°\text{C} < T < -0°\text{C}. \tag{5}$$

The improved cloud microphysics scheme showed the best capability in reproducing the observed variability using an SCM during the TOGA COARE IOP in such parameters as cloud fraction, cloud radiative forcing, and the surface radiative fluxes (Iacobellis and Somerville 2000).

The SCM is forced using data from the TOGA COARE IFA region. Since the model is one-dimensional, large-scale vertical and horizontal advection must be specified from an existing dataset. For our simulations advection data is obtained from the data analysis of Lin and Johnson (1996), as described below.

c. Coupled model

The interaction between the atmosphere and ocean occurs through the transfer of heat, moisture, and momentum across the atmosphere–ocean interface (the skin of the ocean). These fluxes are determined by the state

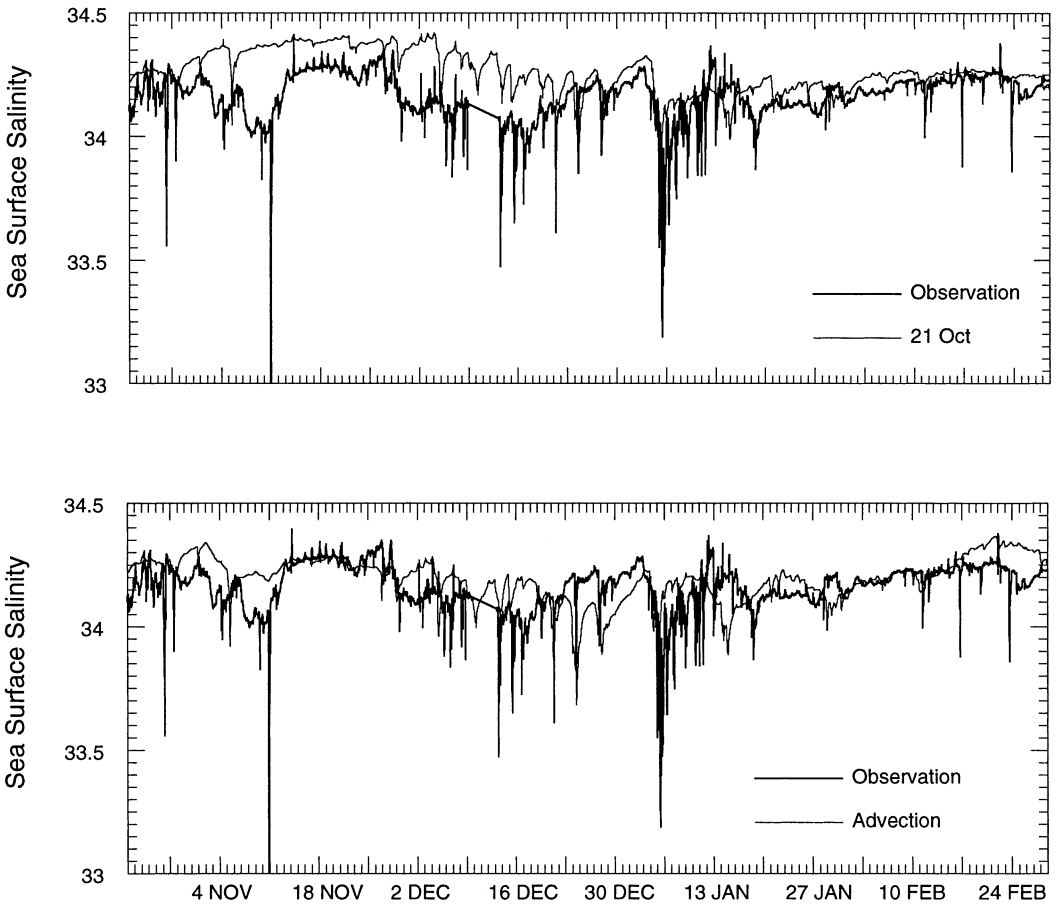

FIG. 2. Observed and modeled SSSs. (top) Model data is from the stand-alone ocean model with no advection and the IMET buoy data for 21 Oct as the initial profile, and (bottom) the stand-alone ocean model with advection and the IMET buoy data for 21 Oct as the initial profile.

of the atmosphere and ocean boundary layers near the interface. These boundary layers are then in turn strongly modified by the surface fluxes. The interface of these boundary layers is the skin of the ocean. The temperature of the ocean skin is a key factor in the exchange of heat and moisture between the ocean and atmosphere. This skin temperature is explicitly calculated within the coupled model (using the Wick 1995 parameterization) and used for the determination of the surface fluxes.

In the coupled model, the atmospheric model provides the near-surface horizontal wind speeds, air mixing ratio, air temperature, precipitation rate, and downwelling shortwave and longwave radiation to the ocean at each time step. These values, combined with the skin surface temperature previously determined by the ocean model, are used as inputs to a turbulent flux model (Clayson et al. 1996). This surface turbulent flux model is internally consistent with the ocean surface layer model incorporated in the Wick (1995) skin surface parameterization. The ocean and atmospheric sublayers are treated consistently with a surface renewal theory based on the work of Brutsaert (1975), in which the renewal timescales of the atmospheric and oceanic sublayers are equivalent to the timescales of the Kolmogorov eddies. The renewal timescale parameterization used in this scheme is consistent with the timescale in the skin model. The modeled turbulent fluxes drive the evolution of the ocean mixed layer. In response to the surface fluxes,

TABLE 1. Cloud population statistics for the atmospheric-only model, and results from the Sheu et al. (1997) analysis.

	Low clouds	Warm cloud	Middle clouds	Cirrus	Cirrus with underlying stratiform	Deep convection
Atmospheric	19.5	24.7	16.5	11.5	23.7	4.1
Coupled	18.7	25.2	17.4	11.4	24.1	3.2
Sheu et al. (1997)	14.8	35.6	22.8	2.5	21.8	2.4

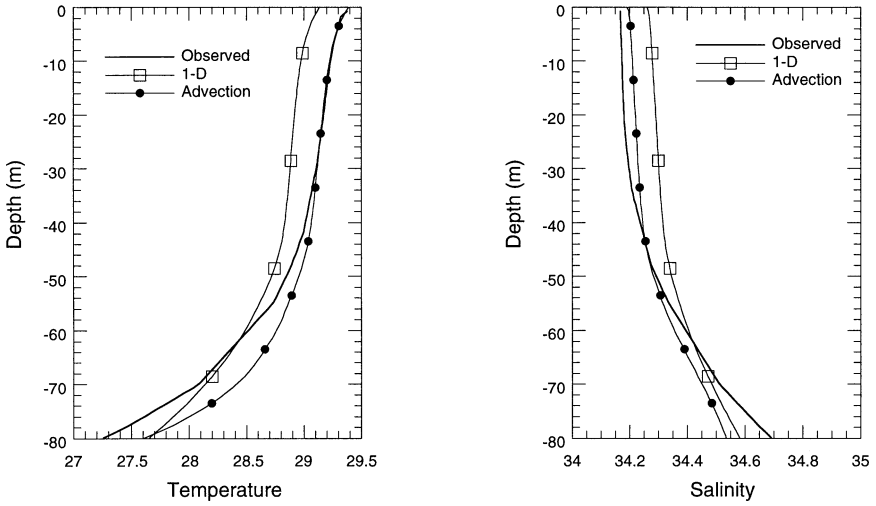

FIG. 3. Average (left) temperature and (right) salinity profiles for the IOP using the stand-alone ocean model with and without advection as compared to observations.

the ocean model determines a new profile of temperature, salinity, and horizontal velocity. The newly determined SST is used to provide the atmosphere model with an updated surface moisture and latent heat flux, sensible heat flux, and upwelling longwave radiation flux.

3. Observational data

Observational data used in this study is from the TOGA COARE IFA (approximately from 4°S to 2°N and from 150° to 160°E) during the IOP (November 1992–February 1993). A complete description of this dataset is given by Godfrey et al. (1998). Observational data is used to initialize the model, force the model at the horizontal boundaries, and to evaluate the simulations. Data used to initialize the ocean model and evaluate the simulated profiles of temperature, salinity, and currents are obtained from a moored buoy. Data used to initialize and evaluate the atmospheric model are profiles of temperature, humidity, and winds obtained from rawinsonde data. Large-scale atmospheric advective tendencies are obtained from an analysis of radiosonde data. Surface temperature, fluxes, and cloud properties are evaluated using analyses determined from satellite data. Details of the individual datasets used in this study are described below.

TABLE 2. Total cloud amount and solar, infrared, and net cloud forcing for the atmospheric-only model, coupled model, and ISCCP-derived values.

	Total cloud amount (%)	Shortwave forcing (W m^{-2})	Long-wave forcing (W m^{-2})	Net cloud forcing (W m^{-2})
Atmosphere-only model	82	−97	60	−37
Coupled model	82	−97	60	−37
ISCCP-derived values	77	−86	42	−44

a. IMET buoy data

Profiles of ocean temperature, salinity, and currents were obtained from the Woods Hole Oceanographic Institution (WHOI) mooring buoy data during the TOGA COARE IOP located at 1°45′S, 156°E (Weller and Anderson 1996). The instrumentation on the mooring line of the buoy contained 11 temperature recorders, 18 conductivity and temperature recorders, 8 current and temperature recorders, and an Acoustic Doppler Current Profiler (ADCP; Weller and Anderson 1996). The uppermost temperature measurement was obtained at a depth of 0.45 m, and the uppermost salinity measurement was at 2.0 m. Standard measurements of surface meteorological variables are available every 1–7.5 min. For simulations of the ocean model in stand-alone format, the surface heat, moisture, and momentum fluxes from the Improved Meteorological Instrumentation (IMET) buoy data were used to force the model. The use of the area-averaged fluxes (obtained from satellite data) would provide a more realistic area-averaged sea surface temperature and salinity; however, forcing the ocean model with IMET surface flux data facilitates the evaluation of the ocean-only simulation against the mooring data.

b. Atmospheric advective tendencies

The dataset used for providing the horizontal and vertical advective tendencies for the atmospheric component of the SCM is from the analysis of Lin and Johnson (1996). This dataset uses all available rawinsonde and satellite IR data collected within the IFA region. Data from research vessels and the IMET buoy are also used within this analysis. The data is available during the 4-month IOP at 6-h intervals with a vertical resolution of 25 hPa. The analysis includes vertical profiles of the horizontal advective fluxes of temperature and moisture,

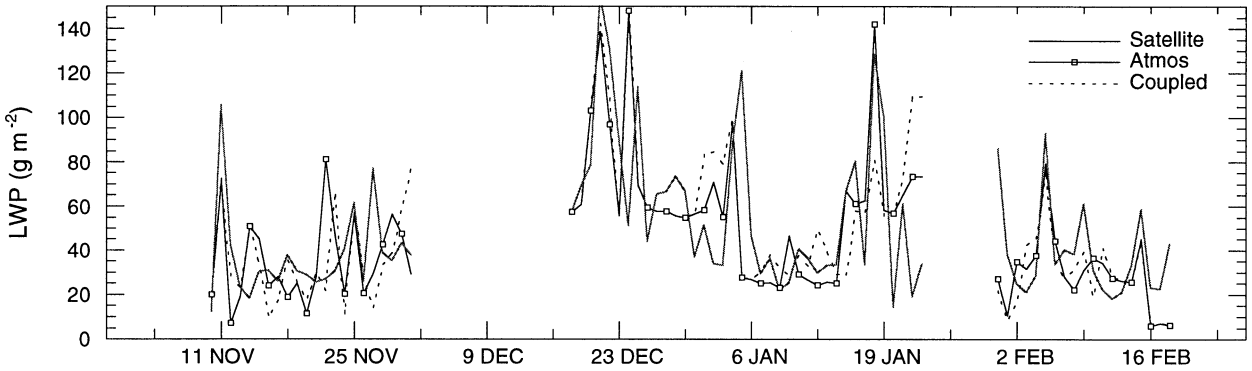

FIG. 4. Time series of column LWP for the atmospheric model, coupled model, and Liu and Curry (1993) satellite-derived dataset.

vertical and horizontal velocities, and temperature and moisture profiles.

Data from the research vessels is an important component of this analysis; there are three separate intervals in which the ships were present: 10 November 1992–1 December 1992, 18 December 1992–23 January 1993, and 31 January 1993–18 February 1993. As in Iacobellis and Somerville (2000), the validation will be almost entirely focused on these three time intervals, as the IFA-averaged values during other time periods do not have the ship data available.

c. Satellite data

Several different satellite datasets are available for evaluation of the model results, including surface temperature, rainfall, surface radiation fluxes, surface turbulent fluxes, surface meteorological variables, cloud optical depth, cloud-top temperature, cloud layer information, cloud liquid water path, and ice water path. The surface flux dataset used in this analysis is described by Curry et al. (1999). This dataset includes all components of the heat, freshwater, and momentum fluxes, as well as other surface variables used in the calculation of these fluxes. The satellite datasets used in this analysis are: the Defense Meteorological Satellite Program (DMSP) Special Sensor Microwave Imager (SSM/I) brightness temperatures, the Advanced Very High Resolution Radiometer (AVHRR) radiances, and the International Satellite Cloud Climatology Project (ISCCP) cloud analysis results. For details of the methodology used, and for a comparison with in situ results, see Curry et al. (1999) and Clayson and Curry (1996). The data is available for the IFA region (from 4°S to 2°N and from 150° to 160°E), with a spatial scale of 50 km and a temporal scale of 3 h. Calculation of the IFA averages uses 78 of these grid areas.

Cloud parameters are determined from the DX version of the ISCCP (Rossow et al. 1996). This analysis, based upon AVHRR and Television Infrared Observational Satellite (TIROS) Operational Vertical Sounder (TOVS) data, provides cloud optical depth, and cloud-top temperature and pressure. Additional cloud information is determined from the cloud analysis of Sheu et al. (1997), which combines the ISCCP with SSM/I. This analysis provides a cloud classification, cloud layer information, and cloud layer liquid water path (LWP) and ice water path. The LWP data is available for the IFA region at pixel-level space–time resolution, which is determined by the SSM/I sampling (approximately twice per day).

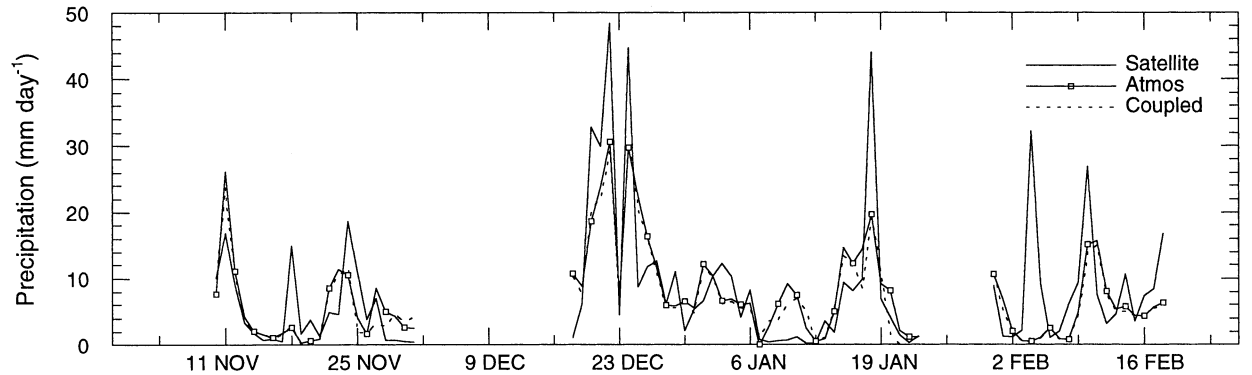

FIG. 5. Time series of daily mean precipitation for the atmospheric model, coupled model, optical rain gauge observations, and the satellite-derived values from Curry et al. (1999).

TABLE 3. Surface heat fluxes from the atmosphere-only model, coupled model, and satellite-derived values.

	Latent heat flux (W m^{-2})	Sensible heat flux (W m^{-2})	Downwelling shortwave flux (W m^{-2})	Downwelling longwave flux (W m^{-2})
Atmosphere-only model	134.0	10.1	240.0	418.0
Coupled model	132.0	10.4	240.1	414.0
Satellite-derived values	106.5	5.3	253.4	425.0

4. Comparison of ocean mixed layer model with observations

The ocean component of the model is run in standalone mode, using atmospheric data from the IMET buoy. The rationale for these simulations is to assess whether discrepancies in the coupled simulations arise from deficiencies in the ocean component of the model. The ocean-only simulations were conducted for the entire 4-month period of the IOP. Two different simulations are conducted: 1) initial data from the mooring and surface forcing from the IMET buoy, but with no advection; and 2) the same simulation as described above, except that horizontal and vertical advective tendencies are included. The rationale for conducting these two simulations is to assess the importance of horizontal and vertical advection. A comparison of model results for the two ocean-only simulations with observations of sea surface temperature (SST) and salinity (SSS) are shown in Figs. 1 and 2; average temperature and salinity profiles of the 4-month period are shown in Fig. 3. The model bias in SST for the simulation without advection is very small until 23 December, during a westerly wind burst, at which time the model begins to cool more dramatically than the observations. Observations of a small portion of the IFA during this time period showed that advection had been a minor factor in the upper-ocean heat content until roughly 20 December (Feng et al. 1998). Prior to this time, the upper-ocean heat content had been little affected by advection, based on results using a Profile Telemetry of Upper Ocean Currents (PROTEUS) buoy in the IFA (Cronin and McPhaden 1997). During the westerly wind burst in late December; inclusion of advection dramatically changes the modeled results. In general the inclusion of advection reduces the SST bias of the 1D model during the periods of the westerly wind burst and later January [during the series of squalls; see Weller and Anderson (1996)]. SSS changes due to advection in the early part of the model period keep the model to approximately the same salinity due to the advective freshening. During the westerly wind burst, advection again plays a large part in the upper-ocean salt content, freshening the upper layer as in the early part of November.

Similarly, the only time period prior to the December westerly wind burst in which the upper-ocean salt content is strongly affected by advection is early November; advection contributes to a freshening of the upper ocean (Cronin and McPhaden 1998). There is a clear bias in the modeled SSS values during the early part of November, which persists until the period of the westerly wind burst. As with the upper-ocean heat content, the upper-ocean salt content is strongly affected by advection during the westerly wind burst (Feng et al. 1998). Following the end of the westerly wind burst at the beginning of January, the western Pacific was subjected to a sequence of periods of low winds and squalls (Weller and Anderson 1996). Several of the periods in which the ocean model results without advection drift (and in which differences between the observed sea surface temperature and the model simulations with advection can be observed) are correlated with the squall periods. During the squalls, sea surface fluxes were similar to values during the westerly wind burst; advection is a likely cause. One such period is 9–13 February.

As expected due to the nature of comparing an ocean model forced by IFA-averaged advection to a point measurement, there are several time periods in which the sea surface temperature differs by 0.2°–0.4°C. One of these periods occurs during the westerly wind burst in late December; the advected heat dramatically changes the modeled results. Sea surface salinity changes due to advection in the early part of the model period keep the model to approximately the same salinity due to the advective freshening. During the westerly wind burst, as noted above, advection again plays a large part in the upper-ocean salt content, freshening the upper layer as in early November. All further results of either the ocean model or the coupled model will refer to the model including oceanic advection. It should be noted that when the ocean model is used within the coupled model, the ocean will be initialized by the IMET buoy profile data from the day on which the simulation is started (see section 3b for details).

5. Comparison of atmospheric and coupled models with observations

Three simulations (corresponding to the three time periods described in section 3b) of both the atmospheric single-column model and the coupled model using the forcing data of Lin and Johnson (1996) and the advection from the 3D ocean model as discussed above were performed. Each of the three simulations was initialized with observed profiles at the appropriate time (for the coupled model this includes the IMET buoy profile data on 10 November, 18 December, and 31 January). Com-

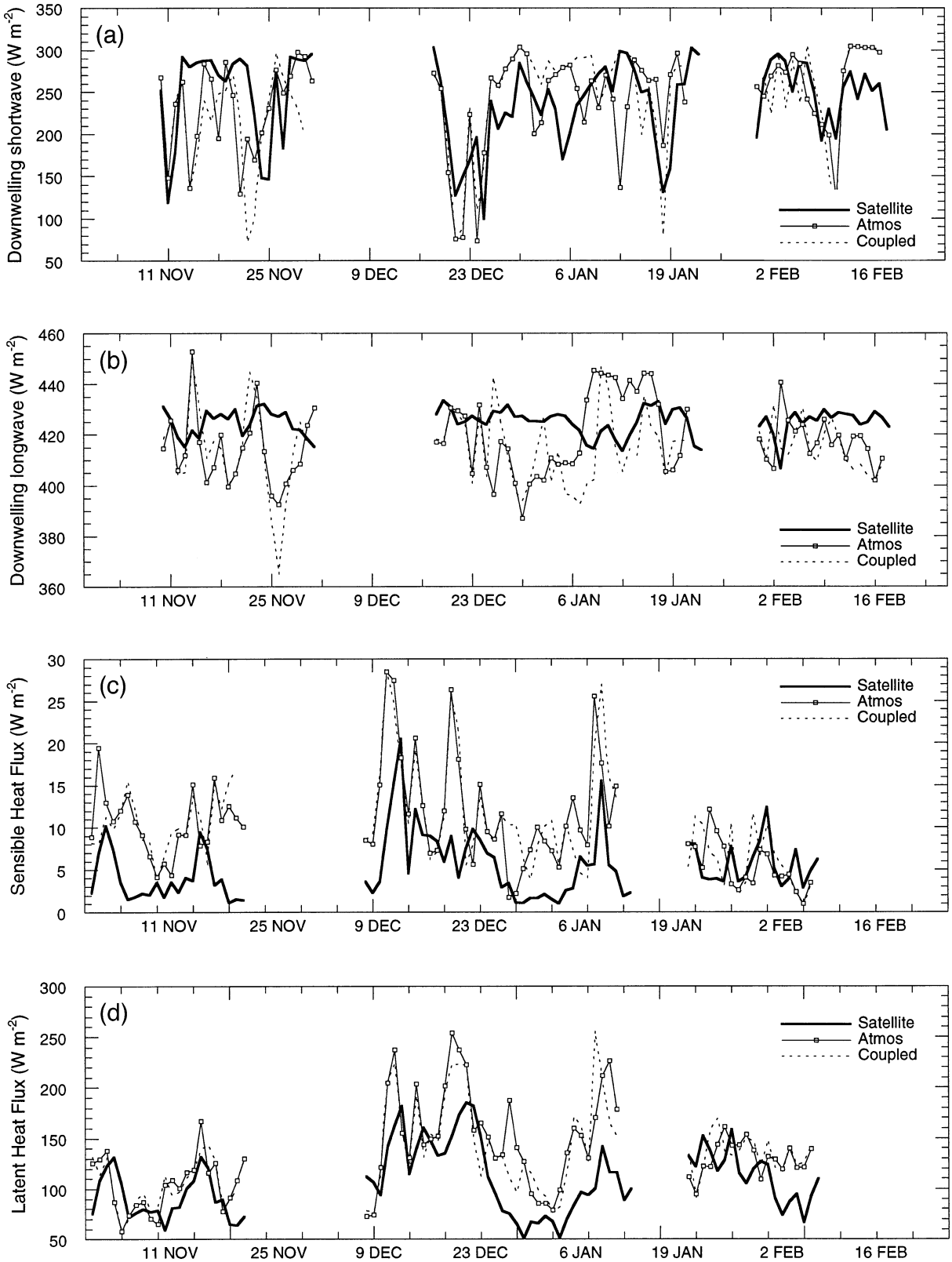

FIG. 6. Time series of daily mean surface heat fluxes from the atmospheric model, coupled model, and the satellite-derived values from Curry et al. (1999). (a) Downwelling surface shortwave radiation, (b) downwelling surface longwave radiation, (c) surface sensible heat flux, and (d) surface latent heat flux.

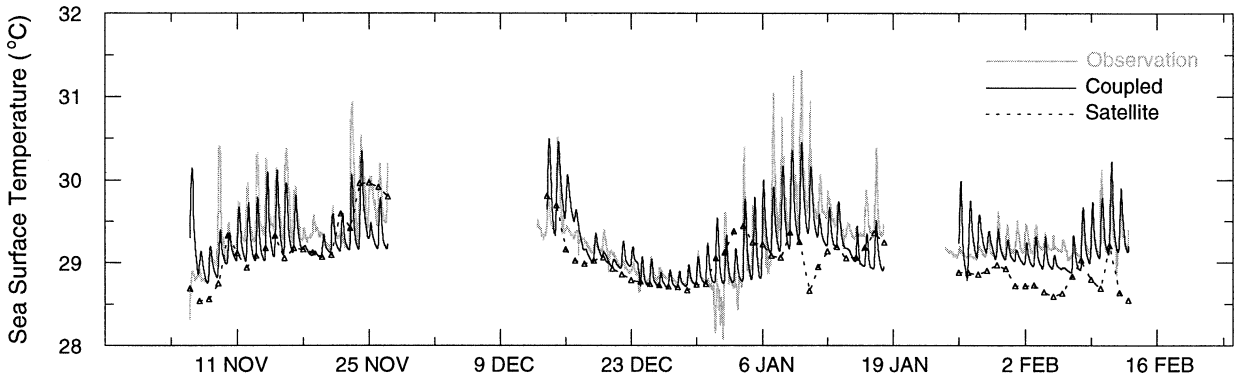

FIG. 7. Time series of SST from the IMET buoy, the satellite-derived IFA average (daily averaged), and from the coupled model.

parisons between model results and various observations are discussed in this section. Since the focus of this model is on examining feedbacks between the ocean and the atmosphere, many of the comparisons will be with quantities that directly affect the sea surface temperature, such as the surface heat, moisture, and momentum fluxes.

a. Mean cloud characteristics

Different cloud types play different roles in the climate system. Large-scale convective clouds provide a strong source of precipitation to the ocean surface, along with increased heat loss due to higher winds and cooler near-surface air temperatures (Young et al. 1995). The regime in which the rain is falling is as important to the upper ocean as is the actual rain amount (Anderson et al. 1996). The main impact of shallower clouds is on the radiative fluxes. Errors in modeled radiative fluxes then may be dependent on the ability of the model to reproduce the vertical distribution and types of clouds. The variability of the cloud water has important effects on the cloud radiative properties, and on precipitation formation within the model. Correct evolution of the sea surface temperature in the coupled model depends critically on the surface fluxes of heat and moisture, which in turn are affected by the cloud characteristics within the model. Information about several types of cloud characteristics is available from satellite observations during the TOGA COARE IOP. The first of these are the cloud population statistics developed by Sheu et al. (1997), as described in section 3c. For this comparison, cloud characteristics are determined from the model based on the effective cloud-top temperature, the effective precipitation rate, and the cloud optical depth. The categories and definitions are the same as those in Iacobellis and Somerville (2000), who used the Sheu et al. (1997) algorithm and results for comparison with their atmospheric single-column model. Comparisons with the Sheu data and this model are shown in Table 1. The model tends to underestimate lower-level clouds and overestimate cirrus clouds. It should be noted that these are frequencies of occurrence of each cloud type, so that the percentages total 100%.

In order to calculate cloud forcing terms, a version of the ISCCP dataset created for TOGA COARE is used (see Rossow et al. 1996). This data is available from 5°S to 5°N and from 150° to 160°E every 3 h with a spatial resolution of 30 km. The total cloud forcing is calculated from

$$\mathrm{CF} = (Q - Q_c) - (F - F_c), \tag{6}$$

where Q is the net incoming solar radiation, Q_c is the net incoming solar radiation in the absence of clouds, F is the outgoing longwave radiation at the top of the atmosphere, and F_c is the outgoing longwave radiation in the absence of clouds. Additional data used for comparison are the cloud-top temperature, the cloud optical thickness, and the cloud-top and cloud-base pressure. Total cloud amount and the solar, infrared, and net cloud forcing results for the atmosphere-only model, the coupled model, and ISCCP-derived values (for the 78 days of the model simulations) are shown in Table 2. Results from the model simulations are identical. Both models overestimate the actual cloud amount as reported by the ISCCP data; the net cloud forcing is less than the ISCCP value, mostly due to a higher longwave forcing value. The values from the models are closer to the ISCCP C1 data reported by Iacobellis and Somerville (2000), with a cloud amount of 73%, a shortwave cloud forcing of -88 W m^{-2}, and a longwave cloud forcing of 50 W m^{-2}. The ISCCP dataset used here differs from the C1 dataset by explicitly treating liquid and ice clouds with different microphysical models (Rossow and Schiffer 1999). Further work is needed toward understanding these differences between the model and the ISCCP data.

The IFA average of LWP from the SSM/I data is shown in Fig. 4, as well as results from the atmospheric and coupled models. The values of LWP from the SSM/I data exclude data from pixels in which the estimated rain rate is greater than 1 mm h^{-1}. Excluding rainy pixels, the IFA-averaged LWP estimate from the SSM/I data during the 78 days of model simulations was 48.9 g m^{-2}, the average from the atmosphere-only model was 47.5 g m^{-2}, and the

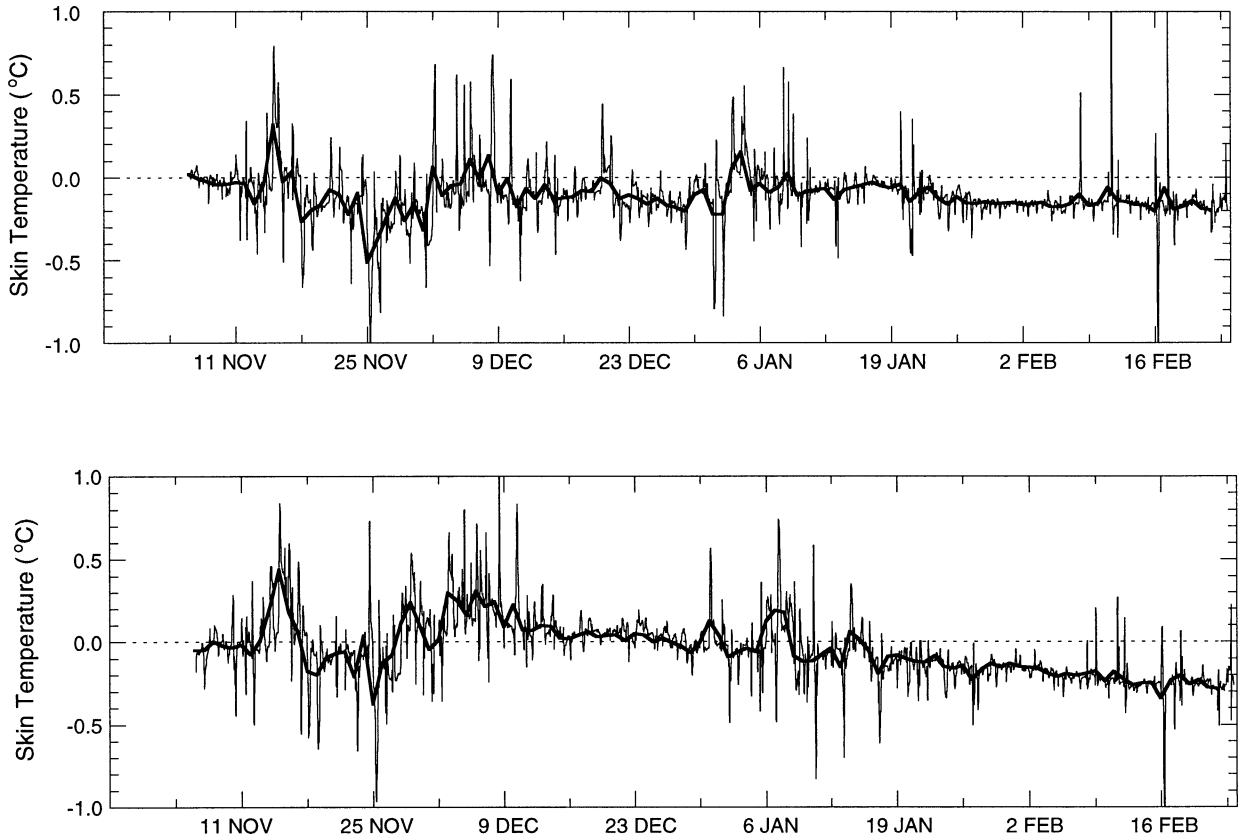

FIG. 8. Time series of skin temperatures from differing simulations. (top) Difference between baseline simulation and simulation with COARE fluxes and (bottom) difference between baseline simulation and CCM3 fluxes simulation. Heavy solid line is daily mean skin temperature.

average from the coupled model was 46.3 g m^{-2}. This discrepancy may be due to the model underestimation of warm and midlevel clouds, as high values of LWP occur during periods of high-, mid-, or low-level cloud fraction in the model (Fig. 18). Differences between the satellite values and the model results are also possibly due to the inclusion in the model results of periods with rain; unlike the satellite data it is not possible to exclude areas of the model domain in which rain is occurring in order to determine a non–rain value. A comparison of LWP between the model and the satellite data is possible when there is no rain in the model; the model again appears to underestimate LWP slightly (as compared to the satellite); the satellite LWP was 31.6 compared to 28.4 g m^{-2} from the coupled model.

b. Precipitation

One of the distinguishing features of the western tropical Pacific warm pool is the excess of precipitation over evaporation that this area receives. The effect of precipitation on the upper ocean is an area of active research (see section 6 for further details). The resulting effects on the atmosphere and feedbacks between the ocean and atmosphere have not been fully quantified. Although some estimates can be made based on the understanding that the existence of a freshwater lens tends initially to decrease the SST (Soloviev and Lukas 1996), a more complete understanding will require a realistic coupled ocean–atmosphere model. The model-simulated values of precipitation must be realistic in order to accurately assess the impacts on the ocean and related feedbacks to the atmosphere. However, accurate measurement of precipitation is a formidable task; according to Godfrey et al. (1998), a 25% uncertainty remains in the surface-based precipitation estimates during the IOP. Comparisons between different data sources are difficult due to the varying spatial scale, as for instance in the comparison between a satellite estimate and a surface measurement (see Curry et al. 1999 for a description of possible sources of discrepancies). Comparison of the results of a single-column model representing a fairly large spatial area with several point measurements within that area is a further source of error.

Comparisons between the atmospheric and coupled model precipitation results and the satellite-derived precipitation dataset of Curry et al. (1999) are shown in Fig. 5. The satellite values have been averaged over the IFA; daily means of the IFA averages are shown. Most

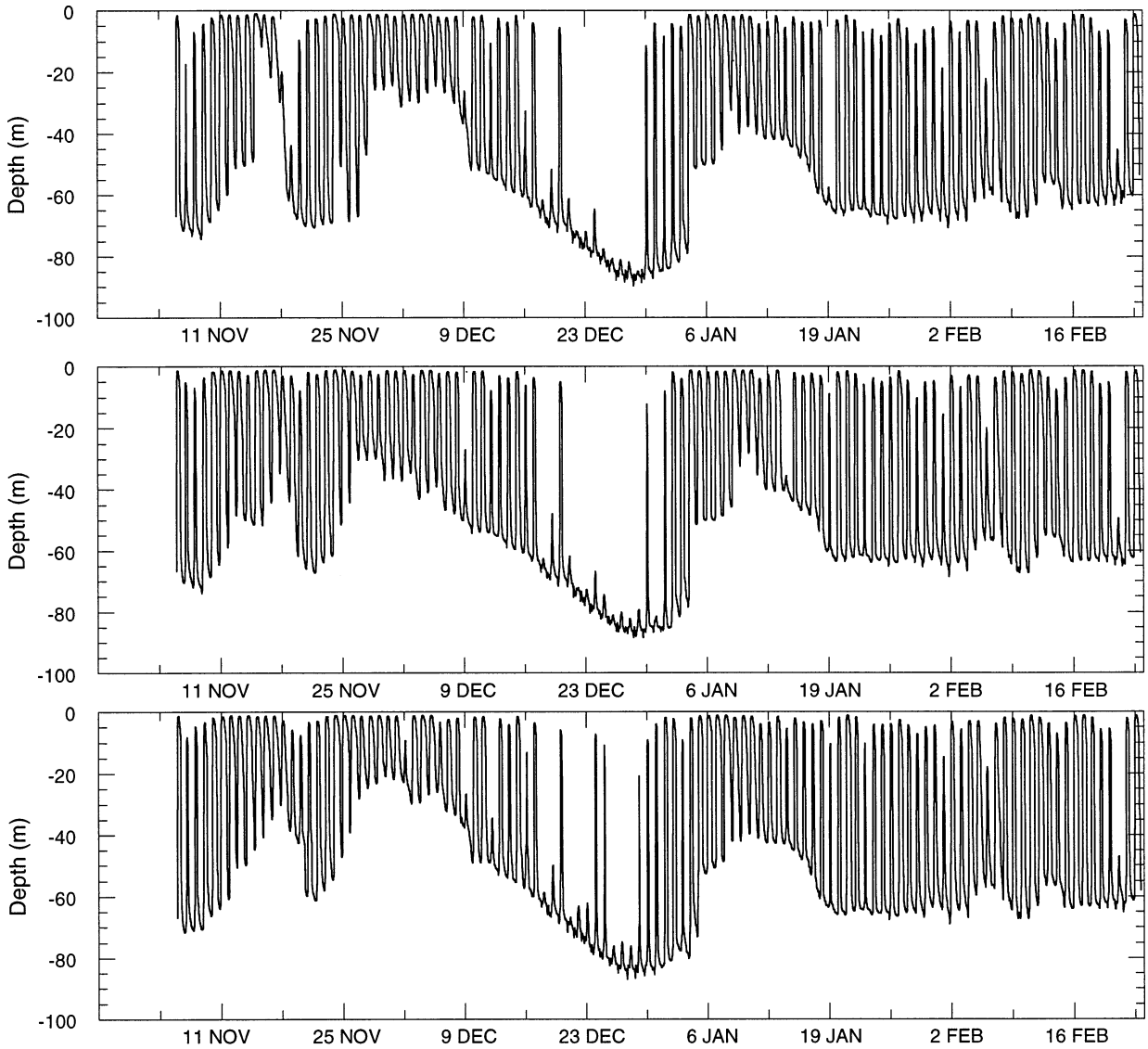

FIG. 9. Time series of the thermocline depth for (top) the baseline simulation, (middle) the COARE flux simulation, and (bottom) the CCM3 simulation.

of the high rain events seen by the satellite are also evident in the model results; there are also some time periods in which the models show rain events that are not evident in the satellite data [but are evident in the optical rain gauge observations as presented by Iacobellis and Somerville (2000)]. The two models show very similar time series, with the coupled model producing slightly smaller values (the mean of the atmospheric model–simulated precipitation is 7.5 mm day^{-1}, the mean of the coupled model–simulated precipitation is 7.0 mm day^{-1}), perhaps due to the underestimation of LWP by the coupled model. The mean satellite-derived precipitation value for the entire IOP is 8.3 mm day^{-1}; averaging the values from the surface rain gauge observational datasets available during TOGA COARE produces a mean of 10.7 mm day^{-1} (Iacobellis and Somerville 2000). Restricting the satellite-derived precipitation values to the 78 days of the model simulations also produces a mean of 8.3 mm day^{-1}. In comparisons of the satellite data with in situ data, Curry et al. found biases of 0.06 mm h^{-1} when compared with data from the optical rain gauge aboard the R/V *Moana Wave*. An IOP average of 8 mm day^{-1} was determined by Feng et al. (1998) as a residual of measured values of evaporation and a determination of the salt budget of the ocean mixed layer.

c. Surface heat fluxes

The tropical western Pacific is a region in which highly accurate surface fluxes are a necessity for determining the sea surface temperature. A commonly stated goal is

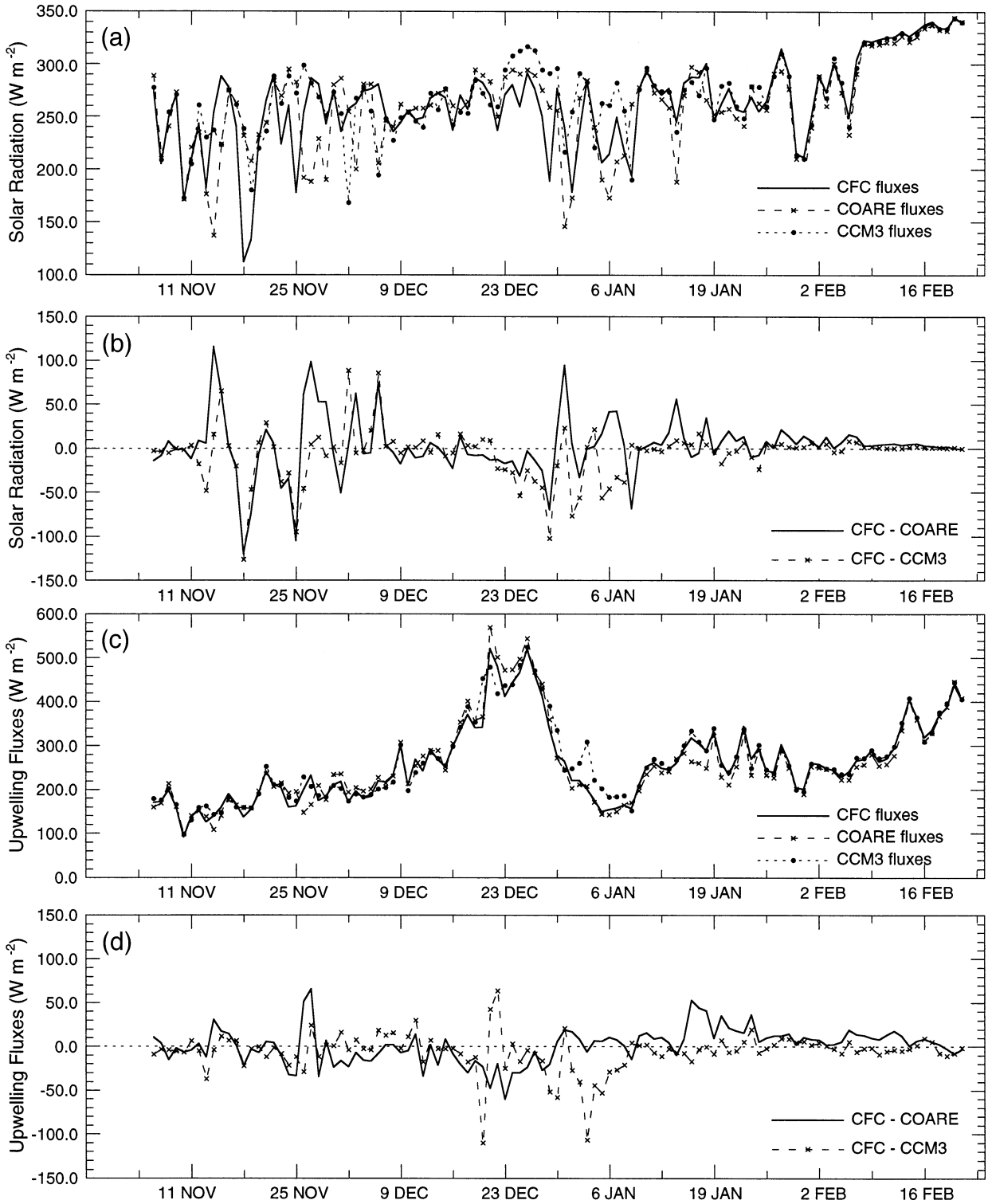

FIG. 10. Time series of the daily averaged (a) surface downwelling shortwave flux, (b) difference in surface downwelling shortwave flux between the simulations, (c) surface net longwave plus latent heat plus sensible heat flux, and (d) difference in surface net longwave plus latent heat plus sensible heat flux between the simulations.

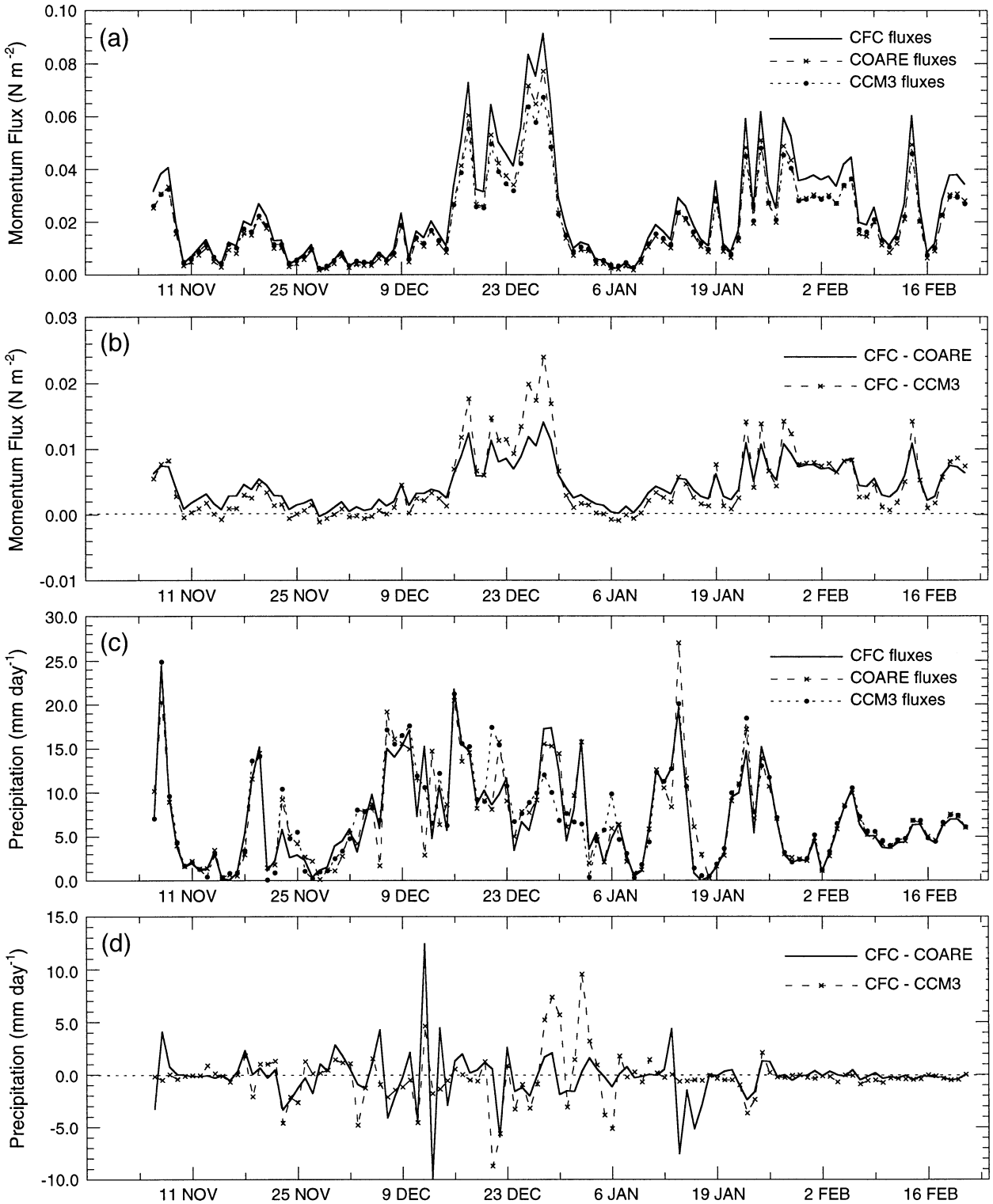

FIG. 11. Time series of the (a) daily averaged surface momentum flux, (b) difference in surface momentum flux, (c) surface rainfall rate, and (d) difference in surface rainfall rate between the simulations.

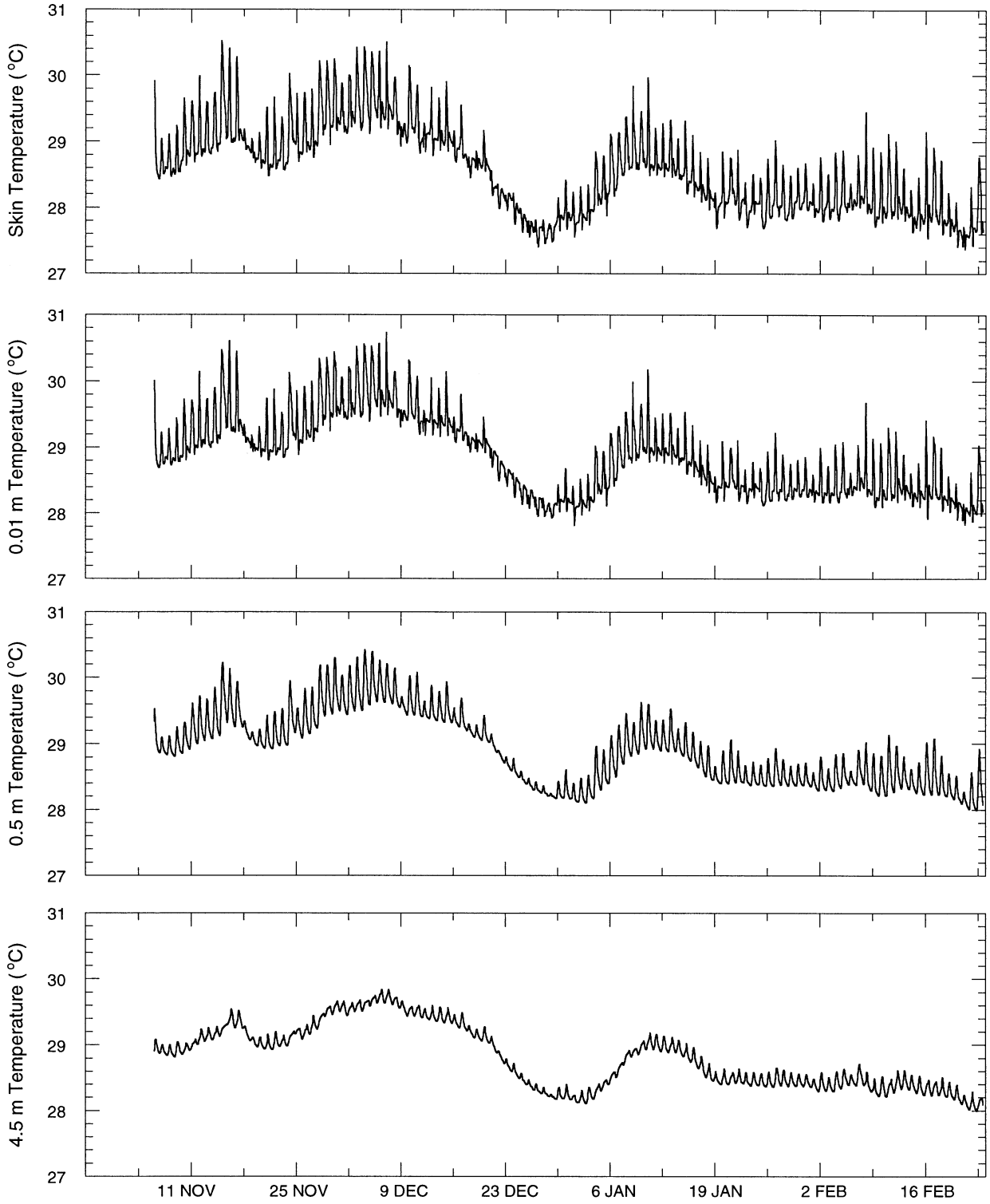

FIG. 12. Time series from the baseline simulation of the coupled model of the skin, 0.01-, 0.5-, and 4.5-m temperatures.

that the surface energy balance of the tropical oceans must be known to within 10 W m^{-2} (e.g., Webster and Lukas 1992). Several studies have examined the total heat flux over parts of the IOP using in situ observations; estimates of the IOP-averaged net surface heat flux made from in situ measurements near the IMET buoy range from 10 to 20 W m^{-2} (Weller and Anderson 1996; Godfrey et al. 1998). Seager et al. (1988) and Gent (1991)

TABLE 4. Fluxes from the baseline simulation (using CFC fluxes), and the simulations using the COARE and CCM3 flux algorithms.

Time period	Solar radiation (W m^{-2})			Surface flux loss (W m^{-2})			Momentum flux (N m^{-2})			Rain rate (mm h^{-1})		
	CFC	COARE	CCM3	CFC	COARE	CCM3	CFC	COARE	CCM3	CFC	COARE	CCM3
All	264	261	270	260	259	266	0.024	0.020	0.020	0.29	0.30	0.30
Nov	229	236	245	168	168	175	0.016	0.012	0.013	0.21	0.21	0.22
Dec	263	261	263	302	316	302	0.028	0.023	0.022	0.38	0.38	0.41
Jan	257	249	268	249	236	263	0.021	0.017	0.017	0.31	0.33	0.30

have shown that a change of 10 W m^{-2} in the net surface heat flux of the tropical western Pacific can change the modeled sea surface temperature by 1°C over a 1-yr period. In a coupled model, the accuracy of the net surface heat flux depends on the accuracy of the radiative and cloud parameterizations in the atmospheric model, the accuracy of the surface turbulent flux model, and the accuracy of the ocean model–produced sea surface temperatures.

The surface fluxes produced by the atmospheric model and the coupled model are shown in Fig. 6. Note that the atmospheric model uses a prescribed SST. For comparison we include the satellite-derived values from Curry et al. (1999) averaged over the IFA region. The satellite-derived surface net heat flux bias at the grid cell nearest the IMET buoy is −19 W m^{-2}; when the data is averaged over a 24-h period the bias is reduced. When using IFA-averaged values, biases were closer to −10 W m^{-2} (satellite biased high). As can be seen from Table 3, the model underestimates the surface shortwave flux and overestimates the fluxes of latent and sensible heat and downwelling longwave radiation compared to the satellite fluxes. Temporal variability is fairly well recreated by the model except for the downwelling longwave radiation; model simulations show much more variability than the satellite values. Differences between the atmosphere-only and coupled model surface fluxes are also evident. These differences tend to occur as distinct events rather than as a general drifting between the two series. This is evident by the close mean values of the fluxes for the two models. The turbulent fluxes appear to be overestimated in the models. Since the wind speed is very close to the observed value, as is the sea surface temperature, the difficulty must lie with the near-surface air temperature and specific humidity. It should be noted that the Clayson et al. (1996) algorithm was used to compute the turbulent fluxes for both the satellite-derived and the model-derived values. Thus differences between the satellite-derived and the model-derived values are not due to differences in the bulk transfer coefficients.

d. Sea surface temperature

The sea surface temperature provides the direct link between the ocean and the atmosphere in the coupled model. Errors in sea surface temperature can be a result of inaccurate surface fluxes (arising from either errors within the atmospheric part of the model or errors in the feedbacks between the ocean and atmosphere) or inaccurate ocean model physics. The sea surface temperature thus provides an indication of the ability of the model to accurately reproduce the natural system, but by itself is not a useful parameter to diagnose inaccuracies within the model.

The SST for the three runs from the IMET observations, satellite data, and the coupled model is shown in Fig. 7. Note that the satellite data is an IFA average value that has been daily averaged for clarity. Since the buoy data is a point observation, the satellite data have been provided to show how the IFA as a whole varied in temperature. The SST from the model generally varies between the values of the IMET buoy and the satellite-derived values. The exception is during the end of December, when the modeled SST stays nearly 0.4°C warmer than either the buoy or the satellite values. This is during a period of strong advection; the three-dimensional model may be overestimating the heat advection. Diurnal variability is fairly realistic, except for the first few days of the third period; an evaluation of the modeled shortwave radiation shows stronger diurnal variability than the observed, perhaps causing the stronger diurnally varying SST. There is no long-term drift in the modeled SSTs. Overall means of SST from the

TABLE 5. Temperatures from a full-model simulation of the TOGA COARE IOP.

	Average temperature (°C)	Average difference from skin temperature (°C)	Average diurnal variability (°C)	Maximum diurnal variability (°C)
Skin	28.56	0	0.83	1.61
0.01 m	28.86	0.30	0.73	1.49
0.5 m	28.91	0.35	0.49	0.90
4.5 m	28.81	0.25	0.20	0.32

TABLE 6. Differences in temperatures for simulations calculating surface fluxes from temperatures at various depths.

Temperature used in surface flux calculation	Average skin temperature (°C)	Average difference from baseline simulation (°C)
Skin (baseline)	28.86	0
0.01 m	28.86	−0.001
0.5 m	28.87	−0.01
4.5 m	28.83	0.03

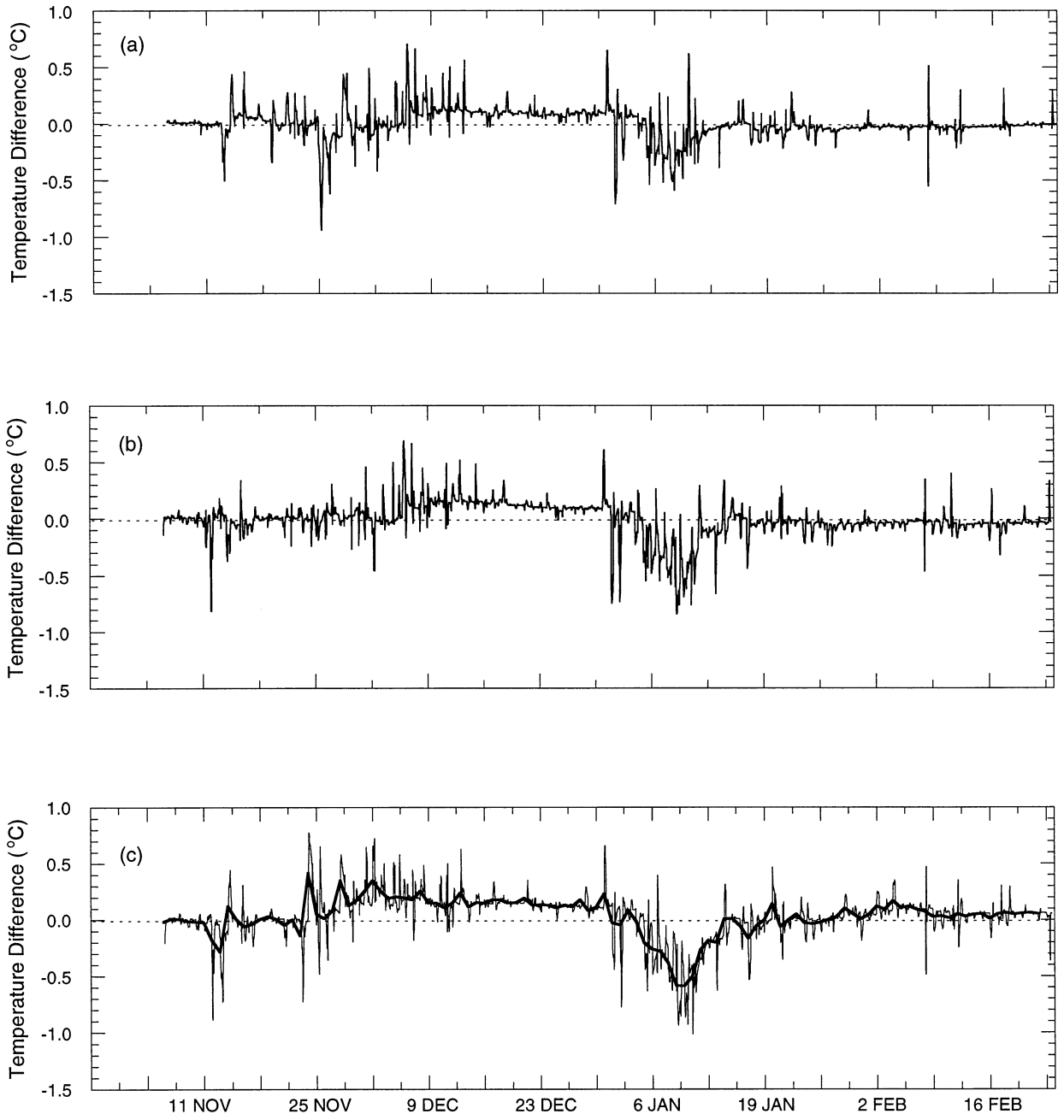

FIG. 13. Time series of skin temperatures from differing simulations. (a) Difference between baseline simulation and 0.01-m temperature simulation, (b) difference between baseline simulation and 0.5-m temperature simulation, and (c) difference between baseline simulation and 4.5-m temperature simulation. Bold line is daily mean temperature difference.

buoy is 29.3°C; the model also has a mean value of 29.3°C, and the satellite data has a mean of 29.1°C.

6. Turbulent flux parameterizations

Given the apparent sensitivity of the tropical ocean–atmosphere system to small variations in surface flux, it is appropriate to determine how sensitive the model is to differing flux parameterizations. A number of different turbulent flux parameterizations have been developed; a recent comparison by BZA outlines differences between most of the available parameterizations. Under conditions typical in the tropical Pacific, differences between the algorithms could result in variations on the order of 20 W m^{-2} in the latent heat flux. In order to evaluate the effects of the surface turbulent flux parameterizations on the coupled model, three flux parameterizations are used. The first is the baseline sim-

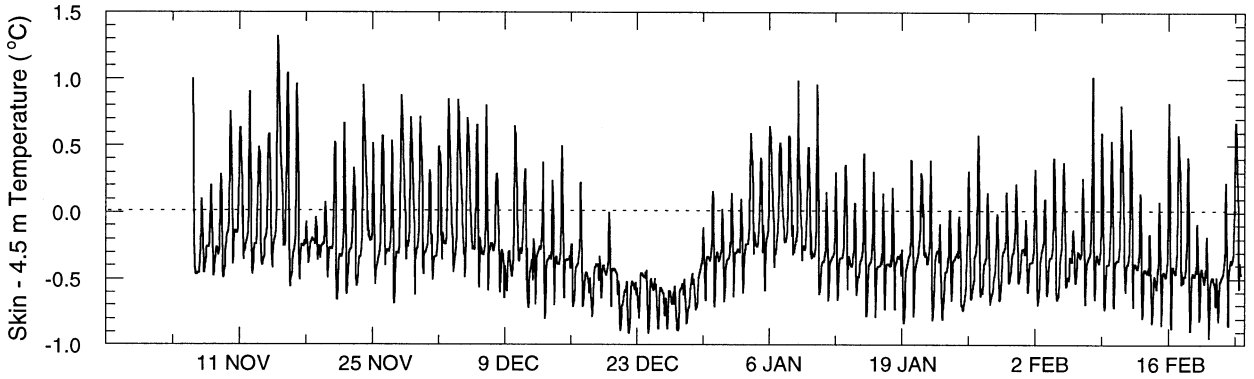

FIG. 14. Time series of difference between skin and 4.5-m temperature in the baseline simulation.

ulation with the turbulent flux model of Clayson et al. (1996) described previously. The second flux parameterization is that of Fairall et al. (1996a), developed using TOGA COARE data (hereafter referred to as the COARE algorithm). The COARE algorithm (like the Clayson et al. algorithm) is based on surface renewal theory, but differs in some key elements in that it uses 1) a different specification of the roughness–stress relationship (with no inclusion of roughness due to capillary waves), 2) a gustiness velocity to account for the additional flux induced by boundary layer–scale variability, and 3) differing roughness lengths for heat and moisture. The third surface flux parameterization used for comparison is that provided with CCM3 (Kiehl et al. 1996).

These three algorithms were shown to have systematic differences in the work of BZA, and as such should give a good indication of the sensitivity of the coupled model to the surface turbulent flux algorithm. The skin temperature differences between the baseline simulation and the simulations using the COARE algorithm and the CCM3 algorithm are shown in Fig. 8. These dif-

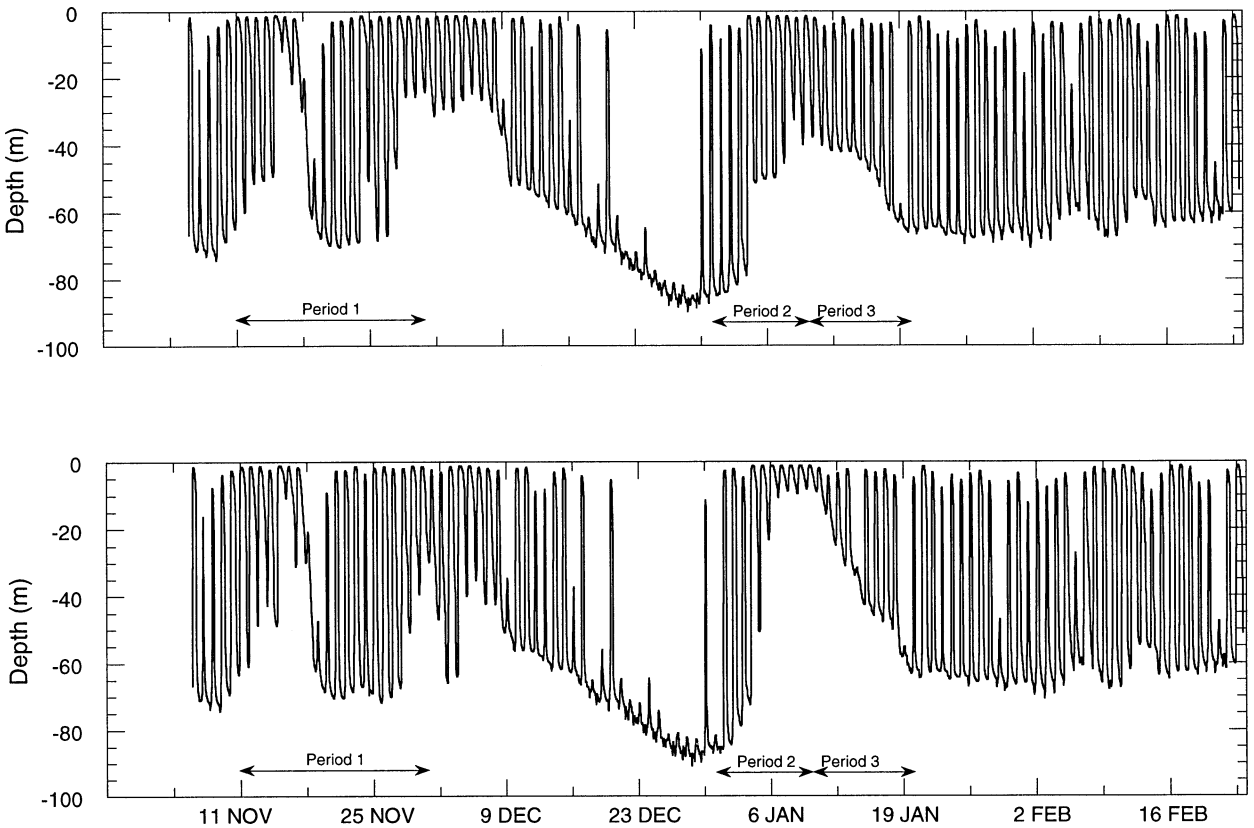

FIG. 15. Time series of the thermocline depth for (top) the baseline simulation, and (bottom) the 4.5-m temperature simulation.

TABLE 7. Fluxes from the baseline simulation and the simulation with the 4.5-m temperature as the interfacial temperature. Surface flux loss is the sum of the net longwave radiation, sensible, and latent heat fluxes. Period 1 corresponds to 13 Nov–2 Dec, period 2 corresponds to 31 Dec–10 Jan, and period 3 corresponds to 11–20 Jan.

	Solar radiation (W m^{-2})		Surface flux loss (W m^{-2})		Rain rate (mm h^{-1})	
Time period	Baseline	4.5-m SST	Baseline	4.5-m SST	Baseline	4.5-m SST
All	264.7	259.4	260.3	258.3	0.29	0.29
Period 1	237.6	217.2	181.4	175.0	0.15	0.15
Period 2	230.5	263.0	189.0	187.0	0.21	0.25
Period 3	275.4	251.6	273.2	259.2	0.27	0.30
All excluding periods 1, 2, 3	276.5	273.1	292.3	293.5	0.34	0.34

ferences between the model simulations can reach nearly 1°C on an hourly basis; daily averaged sea surface temperature differences reached maximum values of 0.5°C. The largest daily averaged SST differences are generally seen during the low-wind periods in November and early December, with slightly smaller differences in early January. Overall there is a bias in SST between the three simulations, with differences between the flux parameterizations causing a 0.2°–0.3°C bias by the end of the simulation.

In general, the simulations and times with warmer sea surface temperatures had shallower mixed layer depths (Fig. 9). For example, the baseline simulation had significantly shallower mixed layer depths during the time period from 11 November to 18 December, when the SST differences between the three simulations were strong. During the latter half of November, the CCM3 simulation tended to have warmer SSTs and shallower mixed layer depths. Differences in mixed layer depths are also apparent in early January.

Surface fluxes for the three simulations are shown in Figs. 10 and 11. The largest differences between the SSTs from the simulations occur during the strongest differences in solar radiation, where daily averaged differences in solar radiation had maximums of over 100 W m^{-2}. Smaller differences are seen in the net longwave, latent, and sensible heat fluxes, although biases between the daily averages can reach 50–100 W m^{-2}. Over the 4-month period, the average biases in surface heat fluxes were roughly 10 W m^{-2} (Table 4), although monthly averages could differ by up to 30 W m^{-2}. Typically the simulations using the Clayson et al. (1996) algorithm (hereafter referred to as CFC), and COARE algorithm produced closer fluxes and SSTs, although under certain conditions the CCM3 results were closer to the CFC. Large biases in solar radiation and other heat fluxes tend to occur concurrently, but not in general at the time periods with the strongest biases in momentum flux or precipitation (Fig. 11). The CFC algorithm consistently produces the highest momentum flux, the strongest bias (as a percentage) seen in any of the surface fluxes. This difference in momentum flux does not produce deeper mixed layers; the differences in mixed layer depths appear to be more sensitive to the cloud (and downwelling shortwave radiation) properties.

7. Sea surface temperature parameterizations

The surface temperature seen by the atmosphere is the skin temperature of the ocean. It is this temperature that determines the surface longwave, sensible, and latent heat fluxes. However, most models use a temperature that comes from other depths in the water column than the actual interfacial temperature. In this section we test the sensitivity of the results of the coupled model to the temperature that is used for determining the upwelling fluxes.

Differences between the temperatures at the skin, at 0.01, 0.5, and at 4.5 m for a simulation in which the coupled model as described above (with the skin temperature determining the upwelling fluxes) is shown in Fig. 12. In this case, the model simulation begins on 10 December 1992 and continues through 28 February 1993. The skin temperature differs from the temperature of the ocean just below the surface ($\sim$1 cm) by $-0.6°$ to $+0.1$°C, due to the heat loss/gain experienced by this thin sublayer (e.g., Schlüssel et al. 1997). For temperatures measured by ships (5-m depth) or buoys (0.5-m depth), the difference from the skin temperature can be even larger, as can be seen in Fig. 12. For temperatures obtained at depths greater than a few centimeters, substantial corrections due to daytime solar heating need to be included (e.g., Fairall et al. 1996b). In addition, at 5-m depth, diurnal variability of temperature is reduced, further changing the calculation of the surface fluxes from those that would be appropriate for the atmosphere. Webster et al. (1996) calculated that for average conditions during TOGA COARE, a 1°C error in SST would result on average in an error in sensible heat flux of 2.4 W m^{-2} (23% of the average value) and an error in latent heat flux of 18.7 W m^{-2} (16% of the average value). Differences between the temperatures at these levels are shown in Table 5. As expected, the skin is generally cooler, and the diurnal variability is greatly reduced at the deeper levels.

In order to evaluate the effects on the coupled system of using the 0.01-, 0.5-, or the 4.5-m temperature as the

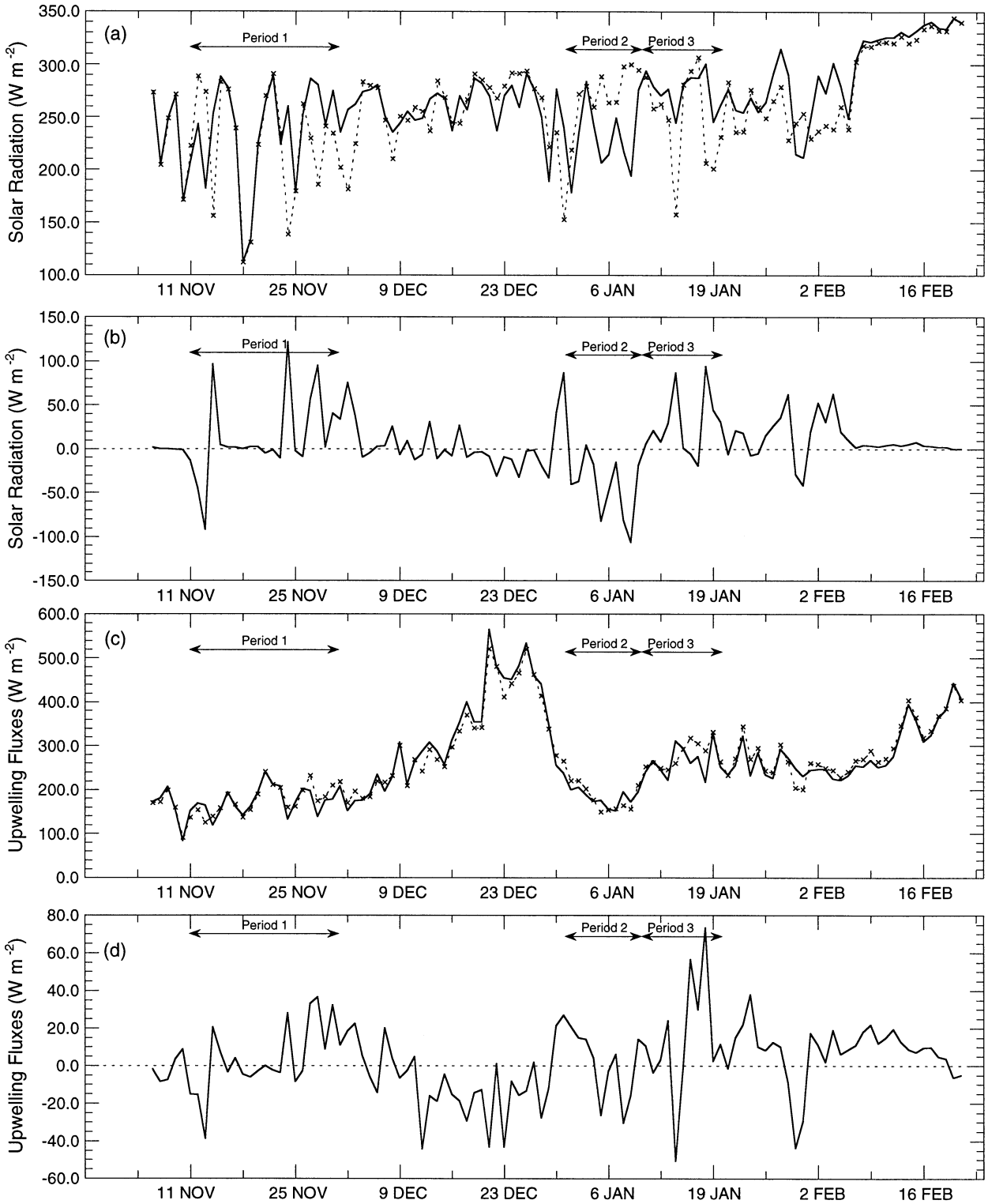

FIG. 16. Time series of the daily averaged (a) surface downwelling shortwave flux, (b) difference in surface downwelling shortwave flux between the two simulations, (c) surface net longwave plus latent heat plus sensible heat flux, and (d) difference in surface net longwave plus latent heat plus sensible heat flux between the two simulations. In (a) and (c) the baseline simulation is shown by a solid line and the 4.5-m temperature simulation is shown by a dashed line.

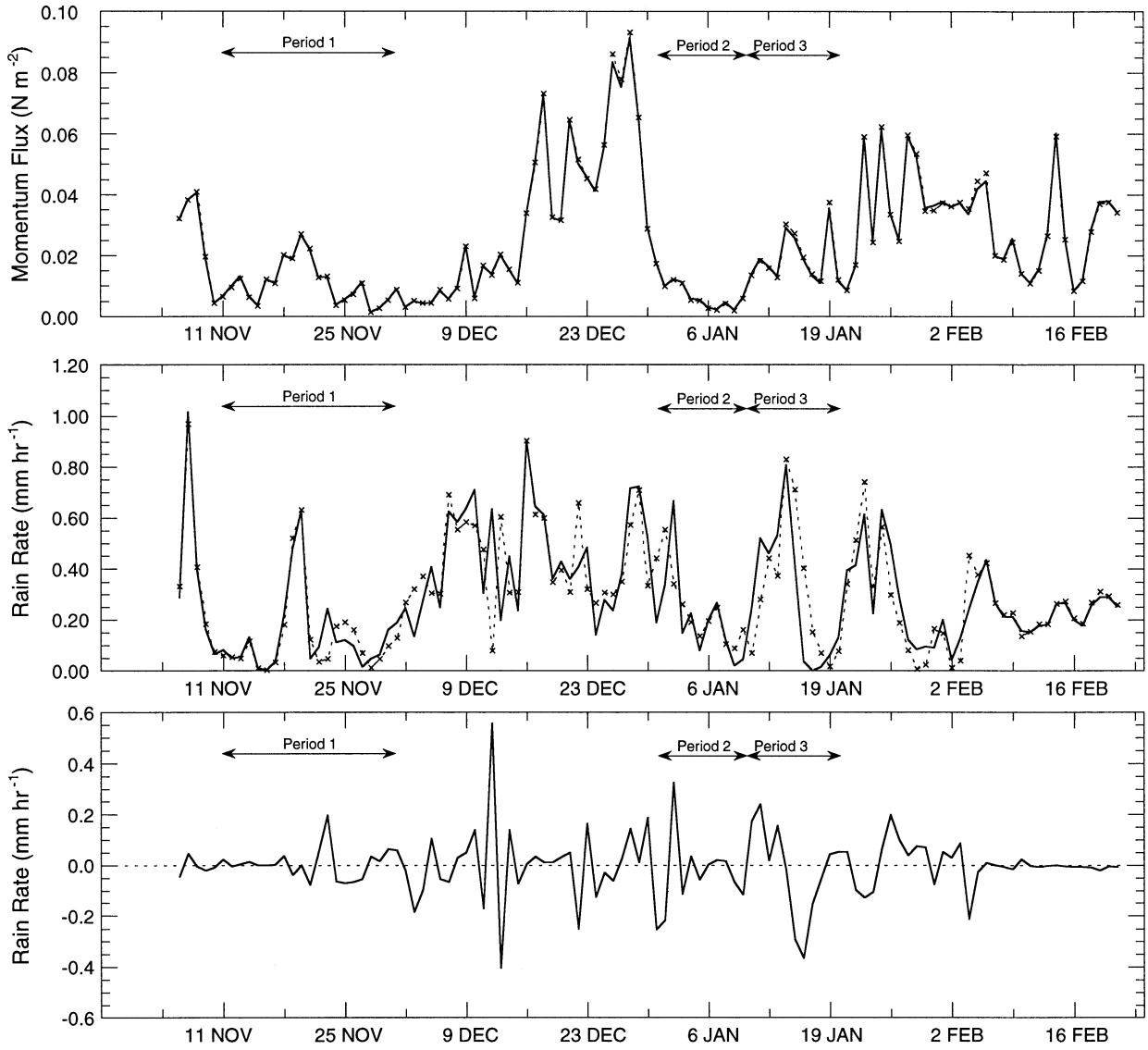

FIG. 17. Time series of (top) the daily averaged surface momentum flux, (middle) surface rainfall rate, and (bottom) difference in surface rainfall rate between the two simulations. Baseline simulation is shown by a solid line and the 4.5-m temperature simulation is shown by a dashed line in the top two panels.

''surface'' temperature, a series of simulations were performed. In each case, all temperatures (including) skin were calculated, but the temperature used for calculating the surface fluxes for coupling to the atmosphere was the temperature from the appropriate depth. The differences in the resulting skin temperatures can be seen in Fig. 13. The average differences (as shown in Table 6) are negligible; there is little discernable long-term bias. The differences in the daily averaged SSTs between the baseline simulation and the simulation using the 4.5-m temperature as the interfacial temperature indicate that there are distinct periods in which the bias between the simulations strongly increases or decreases. The 4.5-m temperature simulation decreases in temperature relative to the baseline simulation twice during this time period, from 13 November to 2 December (period 1) and from 10 to 20 January (period 3). The changes in temperature are approximately 0.6° and 0.7°C, respectively. The 4.5-m temperature simulation also increases its temperature relative to the baseline simulation once, over a 0.8°C range, from 31 December to 10 January (period 2). Very little consistent change in bias is seen outside these three periods. Periods 1 and 3 roughly correspond to the times of low-wind conditions or squalls (Weller and Anderson 1996), while period 2 occurs at the end of the westerly wind burst and the beginning of a light wind period. However, as can be seen in Fig. 14, the largest differences in the baseline simulation between the skin and the 4.5-m temperature were during the westerly wind burst period in mid- to late December. Thus it is not

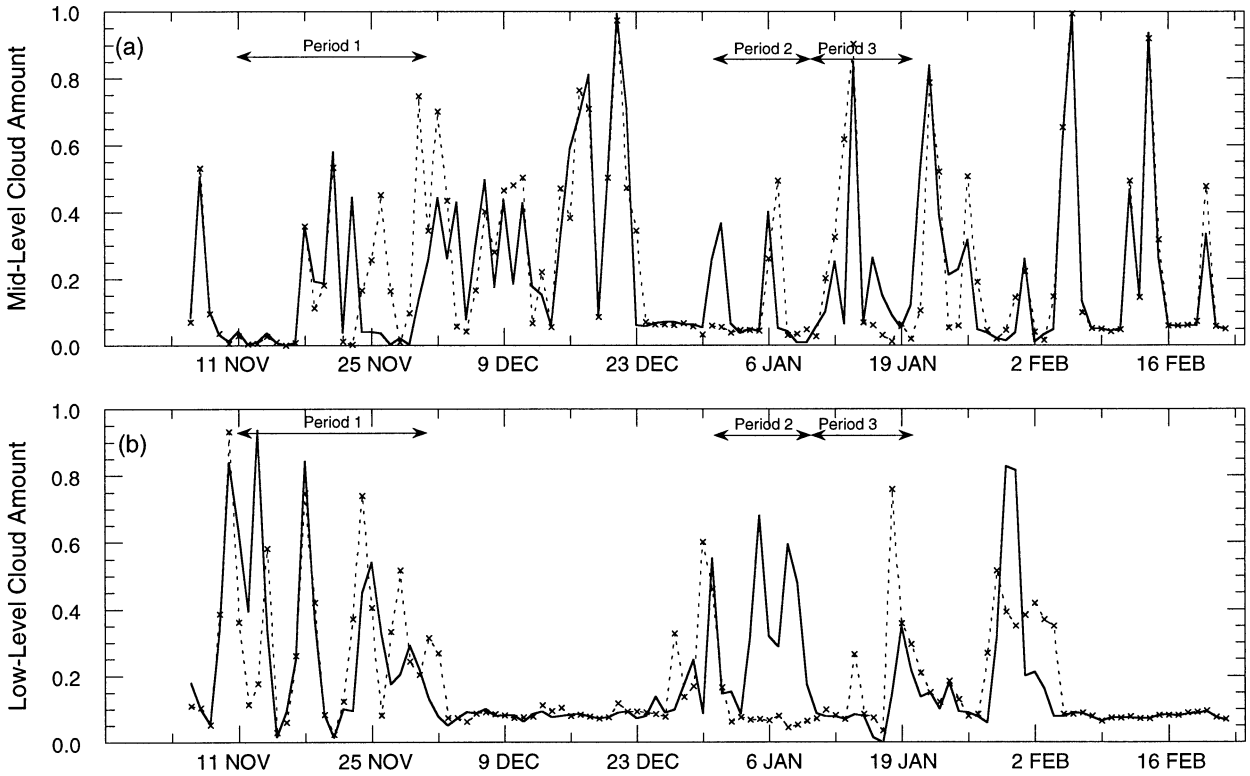

FIG. 18. Time series of (a) the daily averaged midlevel cloud amount, and (b) low-level cloud amount for the baseline simulation (solid line) and the 4.5-m temperature simulation (dashed line).

just the difference between these temperatures causing the differences but feedbacks within the system.

These three time periods also contain the largest differences in thermocline depth (halocline depths were virtually identical in all four simulations). Figure 15 graphically displays the thermocline depths for both the baseline simulation and the 4.5-m temperature simulation. The thermocline depths are nearly identical for the two runs, except during the three periods defined above. When the winds are strong, as during the westerly wind burst event, the mixed layer depths (and the SSTs) are nearly identical. Under light wind conditions however the mixed layer depths can vary substantially. During period 1 the thermocline was deeper in the 4.5-m simulation (33.3 m compared to 29.7 m) on average, which could account for some of the cooling of this simulation relative to the baseline simulation. Changes in the thermocline depth between the two simulations are more apparent in periods 2 and 3; in period 2, the thermocline shallows more rapidly (and remains shallower), which could account for the warming of this simulation relative to the baseline simulation. In period 3, the thermocline in the baseline simulation is deeper initially than the 4.5-m simulation, and does not deepen dramatically. However, the thermocline in the 4.5-m simulation is very shallow initially and deepens dramatically, which is a possible reason for this simulation cooling relative to the baseline simulation. By the end of the period, the thermocline depths for both simulations are equal, and remain so for the rest of the simulation.

Variability in the thermocline depth is dependent on several factors including the surface heat, moisture and momentum fluxes, initial thermocline depth, and temperature differences between the mixed layer and the deeper water. A comparison of the fluxes for the baseline simulation and the simulation with the 4.5-m temperature as the interfacial temperature is shown in Table 7. Surface fluxes from the periods where the bias between the simulations is not varying strongly are nearly identical; during the three periods defined above the solar radiation difference is much larger than the sum of the net longwave and turbulent surface fluxes. In all three periods the momentum flux is identical, indicating that the differences in thermocline depth are not due to changes in wind stress. In two of the periods (period 2 and 3) the 4.5-m temperature simulation has a higher rainfall rate, although the difference is small enough that the halocline depth does not vary between the simulations. As shown in Fig. 16, the three periods occur during times of variable solar radiation, not during periods of consistent high solar radiation. Period 2 also covers the only extended time when the sensitivity simulation has consistently higher solar radiation values, which causes the sharply decreasing mixed layer depth relative to the baseline simulation. None of the three periods occur during periods of high latent and sensible

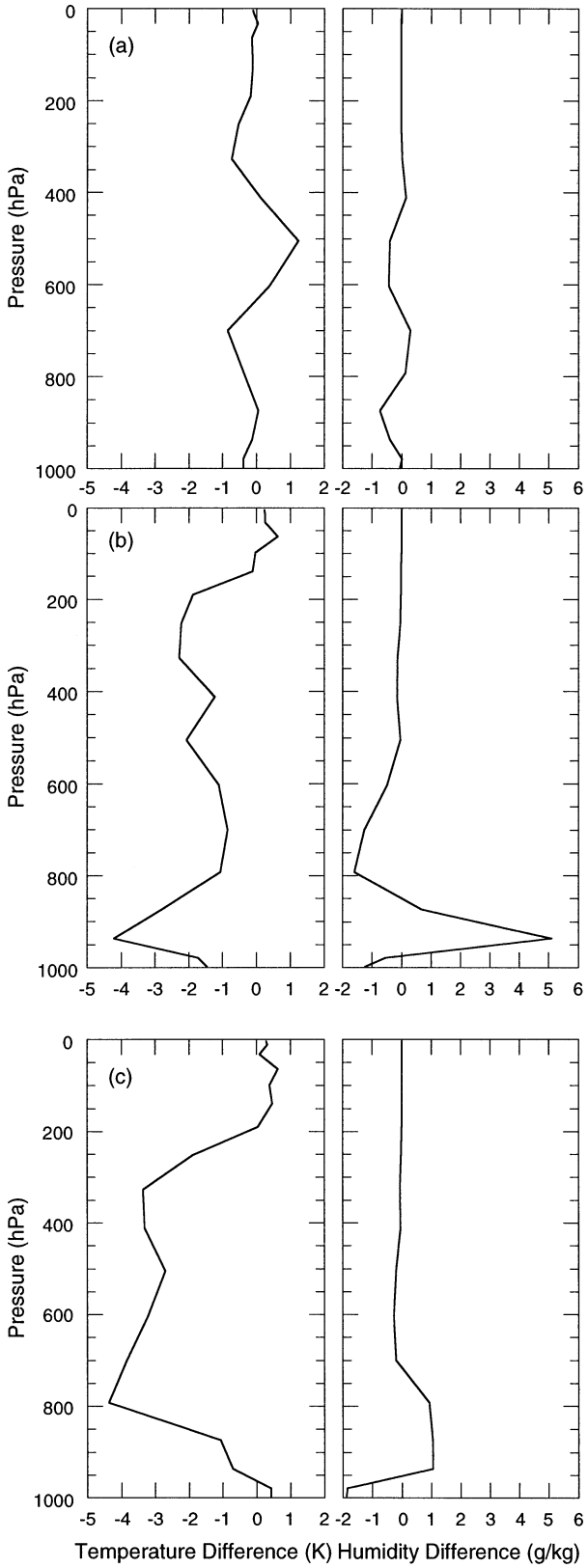

heat flux, which tend to occur during periods of strong winds (Fig. 17). None of the periods with long-lasting increases or decreases in SST bias occurs during periods of strong winds. None of the three periods occurs during conditions of unusual rainfall amounts (either highs or lows), and the changes in rainfall between the two simulations show little effect on the changes in bias (or lack of) from one simulation to another.

Since the bias of the surface solar radiation flux is much greater than the other surface heat fluxes, the momentum flux is little different between the simulations, and the rainfall rates between the two simulations do not vary in a uniform fashion during the three periods; it would appear that the solar radiation is the largest factor in producing the changes in sea surface temperature between the two simulations. The variability in the solar radiation flux is a result of differences in mid- and low-level cloud amounts between the two simulations (Fig. 18). The baseline simulation has significantly lower low-level cloud amounts (defined as clouds below 700 mb) during periods 1 and 3, with higher amounts during period 2, with roughly the same pattern in midlevel (between 700 and 400 mb) cloud amounts, although low-level cloud amount differences are much stronger than the midlevel cloud amounts. The higher cloud amounts in the baseline simulation during period 2 can be seen to be related to much higher moisture content in the lowest 100 mb relative to the simulation with the 4.5-m temperature (Fig. 19). The atmosphere below 900 mb is also cooler in the baseline simulations during this period. Period 1 shows little difference in the temperature and humidity profiles on average; period 3 temperatures are cooler throughout most of the column during the baseline simulation. This cooling may be related to the decreased precipitation in the baseline simulation relative to the sensitivity study. Differences in humidity between the two simulations in period 3 are small. Periods 1 and 3 are similar in that any changes in temperature that occur in the atmospheric column are strongest away from the surface, while during period 2 the most significant differences occur below 800 mb. The greater fraction of low-level clouds in period 2 during the baseline simulation is a result of the much cooler and moister temperatures below 800 mb, while in period 3 the baseline simulation has fewer low-level clouds, with the lowest levels of the atmosphere being on average drier than the sensitivity simulation.

There are two general differences between the SSTs at the skin and at 4.5 m: the skin is on average 0.25°C cooler, and the diurnal variability is much greater at the skin. In order to determine the relative importance of

←

FIG. 19. Average profiles of temperature and humidity differences between the baseline and the 4.5-m simulation. (a) Differences for period 1 (13 Nov–2 Dec), (b) differences for period 2 (31 Dec–10 Jan), and (c) differences for period 3 (10 Jan–20 Jan).

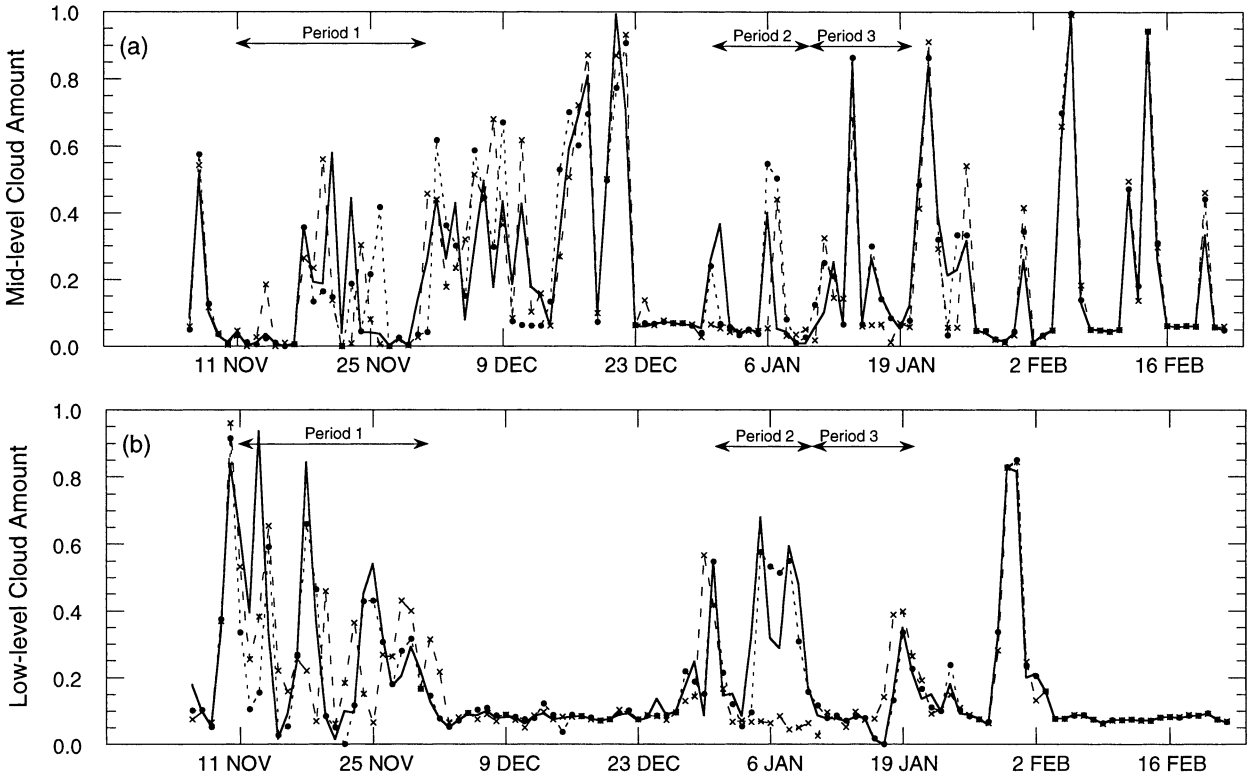

FIG. 20. Time series of (a) the daily averaged midlevel cloud amount, and (b) low-level cloud amount for the 4.5-m simulation (solid line), the warm skin temperature case (dashed line with ×s), and the daily averaged skin temperature (dotted with solid circles).

each of these factors for producing the differences in the simulations seen above, two additional simulations were performed. In both cases, the SST used for calculating the surface fluxes was a given in the model. In the first simulation, the surface temperature was provided by the original skin temperature from the baseline simulation, with a constant 0.25°C warming added. In the second simulation, the original skin temperature from the baseline simulation was averaged for each day (removing all diurnal variability) and then used as the prescribed surface temperature.

Low-level cloud amounts from the baseline simulation and the warmer skin and daily averaged skin simulations (Fig. 20b) during period 1 show that the daily averaged simulation is quite close to the 4.5-m simulation (an average fractional difference of 0.02). However, during period 2, the warm skin simulation is much more similar to the 4.5-m simulation than the daily averaged simulation, indicating that during this time period the cool skin effect is most pronounced. Period 3 is much more complicated, with neither the warm skin nor the daily averaged simulations being similar to the 4.5-m simulation. The results of the midlevel clouds are more complicated; neither of the two sensitivity simulations resemble more closely the 4.5-m simulation than the other, and differences between these simulations average over 10%. Differences in cloud amounts are possibly the result of changes in the temperature and humidity profiles. These differences between the 4.5-m temperature simulations and the warmer skin and daily averaged skin simulations are shown in Fig. 21. As seen in the cloud amounts, during period 1 the daily averaged simulation shows very little difference in the average temperature and humidity profiles, whereas in period 2 the warm skin simulation is nearly identical in temperature and humidity (on average) to the 4.5-m simulation. During period 3 the warm skin simulation has temperature more closely related to the 4.5-m temperature simulation, but the humidity profiles do not clearly indicate that one of these simulations is more like the 4.5-m simulation. From these results, it is clear that both the larger diurnal variability at the skin and the cooler temperature of the skin has an impact on the coupled model. Under certain conditions one of these features may have more of an impact on the coupled system than the other. Certainly low-wind conditions are conducive to strongly varying diurnal SSTs, so the differences between the daily averaged and the actual SST simulations would be strongest at these times. Further feedback analysis may help explain why these differences in the skin temperature have an impact on the coupled model, and under what conditions the cooling of the skin and the strong diurnal variability are important to the coupled system.

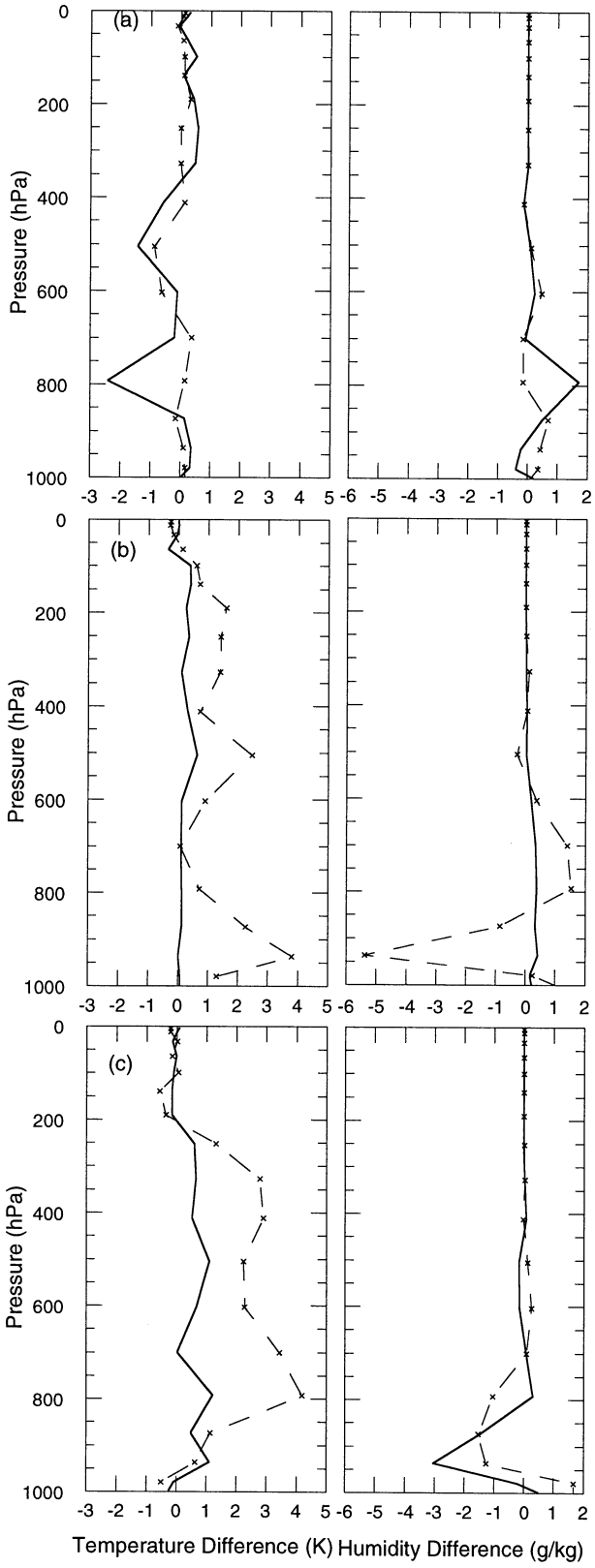

8. Summary

A coupled atmosphere–ocean single-column model has been developed for testing tropical ocean–atmosphere feedbacks and compared with observations during the TOGA COARE IOP. The coupled model is able to successfully reproduce variations in cloud parameters and surface fluxes. The model simulations of surface longwave radiation show much stronger variability than the observed data; the model also overestimates the latent and sensible heat fluxes compared to satellite-derived fluxes. The overestimation is most likely due to errors in the atmospheric surface layer temperature and specific humidity. The sea surface temperatures produced by the model are reasonable. The mean bias in sea surface temperature as compared to buoy data is 0°C; the maximum deviation from the observed temperature is 0.4°C. Some errors in the modeled sea surface temperature may result from the advective tendencies used to force the coupled model.

The sensitivity of the coupled model to the turbulent flux parameterizations was then tested. Short-term variations in both the daily mean surface shortwave and surface turbulent fluxes could reach over 100 W m^{-2}. These translate into significant biases in sea surface temperature, with hourly average differences reaching 1°C on an hourly basis, and daily averaged sea surface temperature differences reaching maximum values of 0.5°C. These sea surface temperature differences appear to be most related to variations in shortwave radiation and its stabilizing influence on the mixed layer depth.

The depth of the ocean temperature used as the sea surface temperature, and the temporal resolution of that sea surface temperature, had as great an impact on the biases between model simulations as did the differing turbulent flux parameterizations. Use of the skin temperature as opposed to a temperature from deeper within the water column produced strong variability in the coupled model during low-wind conditions; the simulations were much more similar during higher wind speeds. These differences were shown to be due to a combination of the use of a consistently warmer sea surface temperature and the lack of diurnal variability, although it appears that these two processes do not equally influence the coupled model at all times.

As noted in the introduction, the single-column model cannot reproduce feedbacks that may occur through nonlocal gradients in ocean temperature or salinity or atmospheric dynamics. Thus the sensitivity of the model

←

FIG. 21. Average profiles of temperature and humidity differences between the 4.5-m simulation, the daily averaged simulation, and the warm skin simulation. (a) Results for period 1, (b) results for period 2, and (c) results for period 3. Differences between the baseline simulation and the warm skin simulation are shown by the solid lines and differences between the baseline simulation and the daily averaged skin temperature simulation are shown by the dashed lines.

to the interfacial parameterizations presents an incomplete picture of the feedbacks within the equatorial Pacific region. However, differences in sea surface temperature of 0.5°C that occur because of differing flux parameterizations, using a temperature occurring within the warmer near-surface water rather than the skin temperature, or ignoring diurnal variability are significant within this climate regime. A more formal feedback analysis for investigating the sensitivity of the model to these parameterizations, and to determine whether these feedbacks are accurate in reproducing the actual climate system, is in progress.

Acknowledgments. We acknowledge with pleasure the support by the NSF under Grants ATM-9629702 and ATM-9629391. We thank Dr. Robert Weller at the Woods Hole Oceanographic Institution for making the IMET buoy data available. We also thank Drs. W. Rossow at NASA GISS for the ISCCP fluxes and G. Liu at The Florida State University for the LWP data. Dr. J. A. Curry provided helpful comments on this paper. Comments by the reviewers also improved the presentation of the paper.

REFERENCES

Anderson, S. D., R. A. Weller, and R. B. Lukas, 1996: Surface buoyancy forcing and the mixed layer of the western Pacific warm pool: Observations and one-dimensional model results. *J. Climate,* **9,** 3056–3085.

Betts, A. K., and M. J. Miller, 1986: A new convective adjustment scheme. Part II: Single column tests using GATE-wave, BOMEX, ATEX, and Arctic Airmass data sets. *Quart. J. Roy. Meteor., Soc.,* **112,** 677–692.

Blumberg, A. F., and G. L. Mellor, 1987: A description of the a three-dimensional coastal ocean circulation model. *Three-Dimensional Coastal Ocean Models,* N. Heaps, Ed., Amer. Geophys. Union, 1–16.

Bourassa, M. A., D. A. Vincent, and W. L. Wood, 1999: A flux parameterization including the effects of capillary waves and sea state. *J. Atmos. Sci.,* **56,** 1123–1139.

Bower, K. N., T. W. Choularton, J. Latham, J. Nelson, M. B. Baker, and J. Jensen, 1994: A parameterization of warm clouds for use in atmospheric general circulation models. *J. Atmos. Sci.,* **51,** 2722–2732.

Brutsaert, W., 1975: A theory for local evaporation (or heat transfer) from rough and smooth surfaces at ground level. *Water Resour. Res.,* **11,** 543–550.

Chen, S. S., R. A. Houze Jr., and B. E. Mapes, 1996: Multiscale variability of deep convection in relation to large-scale circulation in TOGA COARE. *J. Atmos. Sci.,* **53,** 1380–1409.

Clayson, C. A., 1995: Modeling the mixed layer in the tropical Pacific and air–sea interactions: Application to a westerly wind burst. Ph.D. dissertation, Dept. of Aerospace Engineering Sciences, University of Colorado, Boulder, CO, 174 pp.

——, and J. A. Curry, 1996: Determination of surface turbulent fluxes for TOGA COARE: Comparison of satellite retrievals and in situ measurements. *J. Geophys. Res.,* **101,** 28 515–28 528.

——, and L. H. Kantha, 1999: Turbulent kinetic energy and dissipation rate in the equatorial mixed layer. *J. Phys. Oceanogr.,* **29,** 2146–2166.

——, J. A. Curry, and C. W. Fairall, 1996: Evaluation of turbulent fluxes at the ocean surface using surface renewal theory. *J. Geophys. Res.,* **101,** 28 503–28 513.

——, B. Strahl, and J. Schrage, 2002: 2–3-day convective variability in the tropical western Pacific. *Mon. Wea. Rev.,* **130,** 529–548.

Cronin, M. F., and M. J. McPhaden, 1997: The upper ocean heat balance in the western equatorial Pacific warm pool during September–December 1992. *J. Geophys. Res.,* **102,** 8533–8553.

——, and ——, 1998: Upper ocean salinity balance in the western equatorial Pacific. *J. Geophys. Res.,* **103,** 27 567–27 587.

Curry, J. A., C. A. Clayson, W. B. Rossow, G. Considine, G. Liu, R.-S. Sheu, P. J. Webster, and Y.-C. Zhang, 1999: High-resolution satellite-derived dataset of the surface fluxes of heat, freshwater, and momentum for the TOGA COARE IOP. *Bull. Amer. Meteor. Soc.,* **80,** 2059–2080.

Fairall, C. W., E. F. Bradley, D. P. Rogers, J. B. Edson, and G. S. Young, 1996a: Bulk parameterization of air–sea fluxes for the Tropical Ocean–Global Atmosphere Coupled Ocean–Atmosphere Response Experiment. *J. Geophys. Res.,* **101,** 3747–3764.

——, ——, J. S. Godfrey, G. A. Wick, J. B. Edson, and G. S. Young, 1996b: Cool-skin and warm-layer effects on sea surface temperature. *J. Geophys. Res.,* **101,** 1295–1308.

Fasullo, J., and P. J. Webster, 1999: Warm pool SST variability in relation to the surface energy balance. *J. Climate,* **12,** 1292–1305.

Feng, M., P. Hacker, and R. Lukas, 1998: Upper ocean heat and salt balances in response to a westerly wind burst in the western equatorial Pacific during TOGA COARE. *J. Geophys. Res.,* **103,** 10 289–10 311.

Gent, P. R., 1991: The heat budget of the TOGA-COARE domain in an ocean model. *J. Geophys. Res.,* **96,** 3323–3330.

Godfrey, J. S., R. A. Houze Jr., R. H. Johnson, R. Lukas, J.-L. Redelsperger, A. Sumi, and R. Weller, 1998: Coupled Ocean–Atmosphere Response Experiment (COARE): An interim report. *J. Geophys. Res.,* **103,** 14 395–14 450.

Hack, J. J., B. A. Boville, B. P. Briegleb, J. T. Kiehl, P. J. Rasch, and D. L. Williamson, 1993: Description of the NCAR Community Climate Model (CCM2). NCAR Tech. Note NCAR/TN-336+STR, 108 pp.

Holtslag, A. A. M., and B. A. Boville, 1993: Local versus nonlocal boundary-layer diffusion in a global climate model. *J. Climate,* **6,** 1825–1842.

Iacobellis, S. F., and R. C. J. Somerville, 2000: Implications of microphysics for cloud-radiation parameterizations: Lessons from TOGA COARE. *J. Atmos. Sci.,* **57,** 161–183.

Kantha, L. H., and C. A. Clayson, 1994: An improved mixed layer model for geophysical applications. *J. Geophys. Res.,* **99,** 25 235–25 266.

Kiehl, J. T., J. Hack, G. Bonan, B. Boville, B. Briegleb, D. Williamson, and P. Rasch, 1996: Description of the NCAR Community Climate Model (CCM3). NCAR Tech. Note NCAR/TN-420+STR, 152 pp.

Lau, K.-M., and S.-H. Sui, 1997: Mechanisms of short-term sea surface temperature regulation: Observations during TOGA COARE. *J. Climate,* **10,** 465–472.

Levitus, S., 1984: Annual cycle of temperature and heat storage in the world ocean. *J. Phys. Oceanogr.,* **14,** 727–746.

Li, X., C.-H. Sui, D. Adamec, and K.-M. Lau, 1998: Impacts of precipitation in the upper ocean in the western Pacific warm pool during TOGA-COARE. *J. Geophys. Res.,* **103,** 5347–5359.

Lin, X., and R. H. Johnson, 1996: Heating, moistening, and rainfall over the western Pacific warm pool during TOGA COARE. *J. Atmos. Sci.,* **53,** 3367–3383.

Liu, G., and J. A. Curry, 1993: Determination of characteristic features of cloud liquid water from satellite microwave measurements. *J. Geophys. Res.,* **98,** 5069–5092.

Neelin, J. D., 1991: The slow sea surface temperature mode and the fast-wave limit: Analytic theory for tropical interannual oscillations and experiments in a hybrid coupled model. *J. Atmos. Sci.,* **48,** 584–606.

Palmer, T. N., and D. A. Mansfield, 1984: Response of two atmospheric general circulation models to sea-surface temperature

anomalies in the tropical east and west Pacific. *Nature,* **310,** 483–485.
Philander, S. G. H., T. Yamagata, and R. C. Pacanowski, 1984: Unstable air–sea interactions in the tropics. *J. Atmos. Sci.,* **41,** 604–613.
Randall, D. A., K.-M. Xu, R. J. C. Somerville, and S. Iacobellis, 1996: Single-column models and cloud ensemble models as links between observations and climate models. *J. Climate,* **9,** 1683–1697.
Rossow, W. B., and R. A. Schiffer, 1999: Advances in understanding clouds from ISCCP. *Bull. Amer. Meteor. Soc.,* **80,** 2261–2288.
——, A. W. Walker, D. Beuschel, and M. Roiter, 1996: International Satellite Cloud Climatology Project (ISCCP): Description of new cloud datasets. WMO Tech. Doc. WMO/TD-No. 737, World Climate Research Programme (ICSU and WMO), Geneva, Switzerland, 115 pp. [Available from World Climate Research Programme, 41 Avenue Giuseppe-Motta, CP 2300, 1211 Geneva 2, Switzerland.]
Schlüssel, P., A. V. Soloviev, and W. J. Emery, 1997: Cool and fresh water skin of the ocean during rainfall. *Bound.-Layer Meteor.,* **82,** 437–472.
Seager, R., S. E. Zebiak, and M. A. Cane, 1988: A model of the tropical Pacific sea surface temperature climatology. *J. Geophys. Res.,* **93,** 1265–1280.
Sheu, R.-S., J. A. Curry, and G. Liu, 1997: Vertical stratification of tropical cloud properties as determined from satellite. *J. Geophys. Res.,* **102,** 4231–4245.
Shukla, J., 1998: Predictability in the midst of chaos: A scientific basis for climate forecasting. *Science,* **282,** 728–731.
Slingo, J. M., 1987: The development and verification of a cloud prediction scheme for the ECMWF model. *Quart. J. Roy. Meteor. Soc.,* **113,** 899–927.
Smith, R. N. B., 1990: A scheme for predicting layer clouds and their water content in a general circulation model. *Quart. J. Roy. Meteor. Soc.,* **116,** 435–460.
Smith, S. D., 1988: Coefficients for sea surface wind stress, heat flux, and wind profiles as a function of wind speed and temperature. *J. Geophys. Res.,* **93,** 15 467–15 472.
Soloviev, A., and R. Lukas, 1996: Observation of spatial variability of diurnal thermocline and rain-formed halocline in the western Pacific warm pool. *J. Phys. Oceanogr.,* **26,** 2529–2538.
Sundqvist, H., E. Berge, and J. E. Kristjansson, 1989: Condensation and cloud parameterization studies with a mesoscale numerical weather prediction model. *Mon. Wea. Rev.,* **117,** 1641–1657.
Suzuki, T., M. Tanaka, and T. Nakajima, 1993: The microphysical feedback of cirrus cloud in climate change. *J. Meteor. Soc. Japan,* **71,** 701–713.
Tiedtke, J., 1993: Representation of clouds in large-scale models. *Mon. Wea. Rev.,* **121,** 3050–3061.
Vogelezang, D. H. P., and A. A. M. Holtslag, 1996: Evaluation and model impacts of alternative boundary-layer height formulations. *Bound.-Layer Meteor.,* **81,** 245–270.
Wang, B., and X. Xie, 1998: Coupled modes of the warm pool climate system. Part I: The role of air–sea interaction in maintaining Madden–Julian oscillation. *J. Climate,* **11,** 2116–2135.
Wang, Y., W. K. Tao, and J. Simpson, 1996: The impact of ocean surface fluxes on a TOGA COARE convective system. *Mon. Wea. Rev.,* **124,** 2753–2763.
Webster, P. J., 1994: The role of hydrological processes in ocean–atmosphere interactions. *Rev. Geophys.,* **32,** 427–445.
——, and R. Lukas, 1992: TOGA COARE: The Coupled Ocean–Atmosphere Response Experiment. *Bull. Amer. Meteor. Soc.,* **73,** 1377–1416.
——, C. A. Clayson, and J. A. Curry, 1996: Clouds, radiation, and the diurnal cycle of sea surface temperature in the tropical western Pacific. *J. Climate.,* **9,** 1712–1730.
——, V. Magana, T. N. Palmer, J. Shukla, R. A. Tomas, M. Yanai, and T. Yasunari, 1998: Monsoons: Processes, predictability and the prospects for prediction. *J. Geophys. Res.,* **103,** 14 451–14 510.
Weller, R. A., and S. P. Anderson, 1996: Surface meteorology and air–sea fluxes in the western equatorial Pacific warm pool during the TOGA Coupled Ocean–Atmosphere Response Experiment. *J. Climate,* **9,** 1959–1990.
Wick, G., 1995: Evaluation of the variability and predictability of the bulk-skin SST difference with application to satellite-measured SST. Ph.D. thesis, University of Colorado, Boulder, CO, 139 pp.
Young, G. S., S. M. Perugini, and C. W. Fairall, 1995: Convective wakes in the equatorial western Pacific during TOGA. *Mon. Wea. Rev.,* **123,** 110–123.
Zhang, G. J., and N. A. McFarlane, 1995: Sensitivity of climate simulations to the parameterization of cumulus convection in the Canadian Climate Centre general circulation model. *Atmos.–Ocean,* **3,** 407–446.
Zhang, S., A. J. Plueddemann, S. P. Anderson, and R. A. Weller, 2000: Surface fluxes and their influence on sea surface temperature in the western equatorial Pacific during the Coupled Ocean–Atmosphere Response Experiment. *J. Geophys. Res.,* **105,** 6341–6357.